Drexel University

Annual Progress Report: 2012 Formula Grant

Reporting Period

July 1, 2013 – June 30, 2014

Formula Grant Overview

Drexel University received $1,401,259 in formula funds for the grant award period January 1, 2013 through December 31, 2014. Accomplishments for the reporting period are described below.

Research Project 1: Project Title and Purpose

Role of MeCP2 in Pain and its Regulation by microRNAs – The goal of this research is to understand the role of methyl CpG binding protein 2 (MeCP2) in both normal and aberrant nociception. We hypothesize that the reduced pain sensitivity observed in Rett syndrome (RTT) patients results from a decrease in MeCP2 protein, and that a decrease in microRNAs (miRNAs) that bind and repress translation of MeCP2 will cause an increase in MeCP2 levels and thus contribute to pain. By integrating the two epigenetic mechanisms of DNA methylation and miRNAs, studies described here will render insight on how MeCP2 can bring about global gene regulation in a pain state. Our studies can lead to the identification of novel targets, a better understanding and thus innovative approaches for treating pain.

Anticipated Duration of Project

1/1/2013 – 12/31/2014

Project Overview

Decreased pain perception is commonly reported in children with Rett syndrome (RTT), with nearly all cases of RTT caused by mutations in the MECP2 gene. There is a potential relationship between pain severity and specific mutations in the MECP2 gene, with 65% of RTT patients reporting decreased pain and 75% of the patients experiencing abnormal sensitivity. These data from RTT patients suggest normal MeCP2 function is important in modulating pain. This phenomenon of diminished pain perception in RTT patients offers the "proof of concept" for how the methylation marks "read" by MeCP2 protein and the ensuing gene regulatory consequences upon its binding to genomic DNA is critical in pain perception. Several MeCP2 mouse models including those with RTT-associated mutations have been generated.

The objectives of this research are to:
1) Characterize changes in MeCP2 mRNA, protein and miRNAs in DRG from a mouse model of inflammatory pain and naïve T158A knock in (KI) mice

2) Assess mechanical and thermal sensitivity in MeCP2 T158A KI mice at two different ages (pre-symptomatic 6 weeks and post-symptomatic 9 weeks of age) to evaluate pain sensitivity
3) Validate miRNA binding to the 3'UTR of mouse MeCP2 and in vitro confirmation for one chosen miRNA for its ability to regulate endogenous MeCP2 expression
4) Identify regions of the genome differentially bound by MeCP2 in DRG from a pain model and control (or T158A KI and control as an alternate strategy) by ChIP sequencing.

By utilizing rodent models of pain and RTT, we believe our approach can provide mechanistic insight on a) how miRNAs mediate MeCP2 expression in pain and 2) how binding/occupancy of MeCP2 on genomic DNA in DRG bring about gene regulatory consequences mediating downstream gene expression changes resulting in pain. These studies will investigate miRNA mediated regulation of MeCP2 expression and could provide insight on therapeutic utility of miRNAs. Various aspects of previously unexplored avenues in pain research investigated here will increase our understanding of the molecular mechanisms and could lead to better treatment options for patients suffering from pain.

Principal Investigator

Seena K. Ajit, PhD
Assistant Professor
Drexel University College of Medicine
245 North 15th Street, MS 488
Philadelphia, PA 19102

Other Participating Researchers

Ahmet Sacan, PhD – employed by Drexel University
Melissa T. Manners, BS; Yuzhen Tian, BS – employed by Drexel University College of Medicine

Expected Research Outcomes and Benefits

Present treatment options for pain are limited to NSAIDS, opioids, anticonvulsants and antidepressants providing relief to only about 50% of RTT patients, clearly highlighting the unmet medical need for such a common and widespread ailment. The pain field can benefit from new approaches rendering novel perspectives on how we treat pain. Though disease states are often the result of altered gene expression caused by mutations within a gene, aberrant epigenetic modifications of the chromatin surrounding the gene can also result in profound changes in gene expression. Epigenetics encompasses heritable alterations in gene expression and chromatin without accompanying changes in the DNA sequence. Epigenetics has been predicted to play a key role in pain and analgesia both in terms influencing pro- and anti-nociceptive gene expression and in modulating pharmacodynamics or pharmacokinetic properties of analgesics. Rett is an unusual model to study pain. Our data indicating a miRNA mediated regulation of MeCP2 in rodent models of pain led to the formulation of the hypothesis linking an increase in MeCP2 to pain. Studies during this project will render insight on how a master regulator can bring about global gene regulatory changes under pain state. Our studies also integrate functional

consequences of two different epigenetic mechanisms, DNA methylation and miRNA mediated gene silencing underlying pain. By utilizing rodent models of pain and RTT, we believe our approach can provide mechanistic insight on the role of miRNA mediated MeCP2 expression and its role in pain. Binding/occupancy studies of MeCP2 on genomic DNA in neuronal tissue will help elucidate the gene regulatory consequences mediating downstream gene expression changes resulting in pain.

Summary of Research Completed

Aim 1 Characterize changes in MeCP2 mRNA, protein and miRNAs in dorsal root ganglion (DRG) from a mouse model of pain and naïve T158A transgenic mouse.
We purified total RNA from dorsal root ganglion (DRG) from 1) mice four weeks after spinal nerve injury (SNI model mice-a rodent model of neuropathic pain), 2) naïve T158A transgenic mice and 3) naïve Mecp2 null mice.

We performed miRNA profiling of DRG from Mecp2 null mice and prioritized it over T158A mice and SNI model mice to investigate whether the loss of MeCP2 modulates miRNA expression in DRG. This data will enable us to examine the role of altered miRNAs in mediating expression of genes relevant to pain. miRNA profiling of DRG from 11 to 12 week-old postsymptomatic Mecp2 null mice identified 2 upregulated and 17 downregulated miRNAs that were significantly different from control samples (Fig. 1 & Table 1). miR-200c showed a 556-fold upregulation in DRG from Mecp2 null mice. Some miRNAs including miR-200c are predicted to target Mecp2 3′UTR, suggesting feedback loop–mediated regulation of MeCP2 and miRNAs. We performed a luciferase assay and confirmed that miR-200c can indeed bind the 3′UTR of Mecp2 (Fig. 2).

Aim 2 Assess mechanical and thermal sensitivity in MeCP2 T158A KI mice.
Several Mecp2 mouse models, including those with RTT-associated mutations, have been generated. Mecp2-mutant mice have several behaviors reflecting human RTT symptoms, including repetitive forelimb movements resembling stereotypical hand movements, decreased motor function, abnormal social behaviors, and abnormal respiratory patterns. Based on the observation of decreased pain sensitivity in patients, we hypothesized that MeCP2 may play an important role in the development and/or maintenance of pain. T158A mice appear normal at birth and are presymptomatic until 5 weeks of age when neurological symptoms develop. Observing decreased pain sensitivity in these mice will confirm our hypothesis that MeCP2 plays a role in mediating pain sensitivity and confirm the functional implication of a mutation in the methyl binding domain. Sensitivity to mechanical stimuli and thermal hyperalgesia was assessed using von Frey filaments and a Hargreaves test on each hind paw. Procedure for von Frey testing was described in the previous report. For Hargreaves test, the baseline latencies were set to approximately 10 seconds with a maximum of 20 seconds as the cutoff to prevent potential injury. The latencies were averaged over 3 trials separated by 15-min intervals. Our data indicate that T158A knock-in mice have reduced mechanical sensitivity after they develop the RTT-like phenotype. This increase in mechanical pain threshold begins after 11 weeks and persists with age (Fig. 3A). We did not observe an alteration in thermal pain threshold (Fig. 3B).

Aim 3a Validate miRNA binding to the 3'UTR of mouse MeCP2 and confirm miRNA alterations

can modulate endogenous MeCP2 expression in vitro.
Completed and reported in the previous progress report.

Aim 3b To investigate if miRNAs can regulate endogenous MeCP2 expression, we will perform in vitro overexpression and knockdown studies for one miRNA, potentially miR-132.
We used a luciferase reporter assay to validate miRNA binding to the MeCP2 3'UTR and our data demonstrated binding of miR-19, miR-301 and miR-132. We transfected Neuro2a mouse neuroblastoma cells with miRNA precursor, miRNA inhibitor and appropriate controls to verify the reduction of endogenous MeCP2 using western blot analysis. Our data indicates that miRNAs confirmed to bind to the MeCP2 3'UTR also modulate MeCP2 expression (Figure 4). Transfection of miR-301, miR-132, and miR-19 reduced expression of MeCP2, and transfection of miR-301 and miR-132 inhibitors increased MeCP2 expression. Thus, our data suggests that increased expression of miRNAs that target MeCP2 disrupts translation of MeCP2, and inhibitors of endogenous miRNAs block this regulatory mechanism (Figure 4). We also included miR-200c identified from our miRNA profiling of Mecp2 null mice (Aim 1) in these studies.

Aim 4 Identify regions of the genome differentially bound by MeCP2 in DRG from a pain model and control by chromatin immunoprecipitation (ChIP) sequencing.
DNA methylation is a dynamic modification and this reversible biological signal is read by MeCP2. Depending on its interacting protein partners and target genes, MeCP2 can act either as an activator or as a repressor. Alterations in MeCP2 expression and its binding can thus play a critical role in global gene expression in a pain state. Employing genome-wide ChIP-seq can thus provide insight into the function of MeCP2 in contributing to neuropathic pain by highlighting the dynamic relationship between MeCP2, miRNAs and target genes. While investigating the inverse correlation between miRNA and MeCP2, we observed upregulation of MeCP2 protein in DRG from an SNI model of neuropathic pain and a significant decrease of protein in the dorsal horn (reported in the previous progress report). The quantitative differences in MeCP2 protein in dorsal horn and DRG and resulting alterations in chromatin binding could influence gene expression differently in these two tissues in a neuropathic pain state. MeCP2 can induce compaction-related changes in nucleosome architecture as previously reported in brain. We performed ChIP-sequencing using DRG and included dorsal horn for comparative studies.

We developed our ChIP protocol by extensively optimizing published protocols. Reagents from the truChIP tissue chromatin shearing kit (Covaris; Woburn, MA) were used to ensure appropriate fixation and shearing conditions and Millipore (Billerica, MA) magna ChIP G tissue kit reagents were used for immunoprecipitation. L4, L5, and L6 DRG and dorsal horn were collected 4 weeks after SNI or sham surgery and were stored at -80˚C. Each sample was generated by using pooled tissue from 10 mice. DRG samples were intact and dorsal horn was cut into approximately 1-2mm pieces. All downstream steps including sequencing were performed for biological replicates. Protein was cross-linked to DNA using Covaris fixing buffer solution with 1% methanol-free formaldehyde for 5 min, after which the reaction was quenched using Covaris quenching buffer. Tissue was homogenized and cells were lysed in Covaris lysing buffer, and the nuclei were pelleted at 1700xg for 5min. Nuclei were resuspended in Covaris shearing buffer and the Covaris M220 Focused-ultrasonicator was used for efficient and reproducible shearing of chromatin. Our optimization experiments determined that an 11min treatment in the Covaris M220 would yield approximately 200bp chromatin fragments, the ideal

length for ChIP-seq. Before immunoprecipitation, 5ul of each sample was reserved for sequencing input samples, which represent sheared chromatin fragments before immunoprecipitation and was used for normalization of immunoprecipitated samples. Millipore protein G magnetic beads were added to each sample, along with either 5 µl of anti-MeCP2 antibody (gift from our collaborator Dr. Zhou) or 5 µl of rabbit serum (negative control) and incubated overnight. Immunoprecipitated samples were eluted from beads according to Millipore protocol. Protein-DNA crosslinking was reversed and the DNA was purified to remove chromatin proteins as recommended by Millipore. DNA quality and concentration was determined using a Bioanalyzer and samples were submitted for sequencing. Comparative analysis of the sequencing data obtained from SNI and sham from DRG revealed 6 genes and 2 miRNAs with enriched MeCP2-bound chromatin (Table 2). This differential binding in the SNI model suggests that expression of these genes and miRNAs could be regulated by MeCP2 under pain states. Analysis of ChIP-seq data from dorsal horn samples is ongoing.

Figure 1

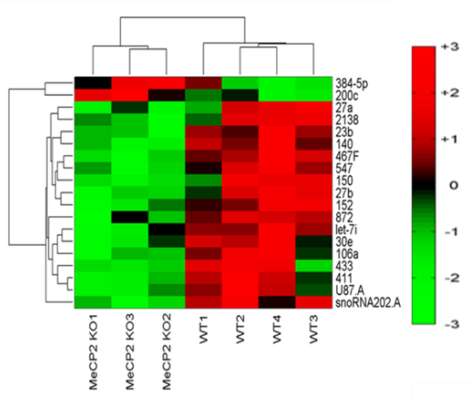

Figure 1 Heat map representation of 19 dysregulated miRNAs (17 downregulated and 2 upregulated) in DRG from Mecp2 null mice at the symptomatic stage (90 days). Red and green indicate high and low expression levels, respectively. See Table 1 for fold change in expression and P values.

Figure 2

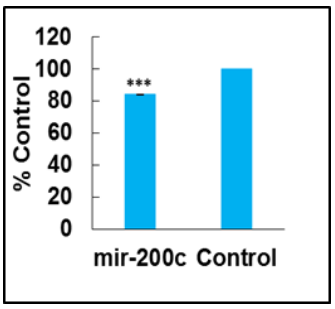

Figure 2. Luciferase reporter assay showing miR-200c can bind to the 3'UTR of Mecp2. The 3'UTR of Mecp2 was cloned downstream of the luciferase open-reading frame. The luciferase activity was measured 24 hours after transfection with miR-200c and the luciferase-UTR plasmid. Data expressed as percentage of control. Statistically significant difference calculated using a Student t-test *** P value <0.001

Figure 3A

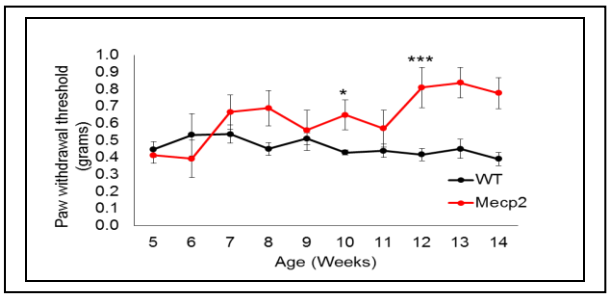

Figure 3B

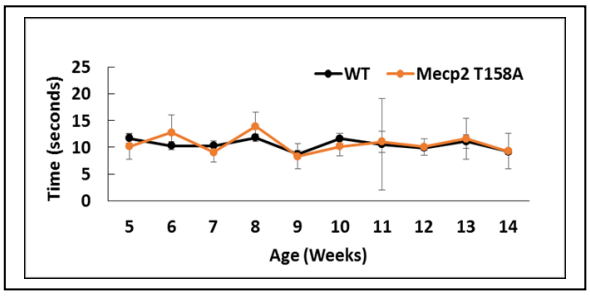

Figure 3 Mecp2 T158A transgenic mice have decreased mechanical (A) but normal thermal sensitivity (B). Mecp2 T158A transgenic mice were assessed for mechanical and thermal sensitivity. Mechanical sensitivity was measured by von Frey filaments and thermal sensitivity was measured with Hargreaves direct heat source. Animals were tested once per week, averages shown from both hind paws are n=3-8 for Mecp2 T158A mutant mice and n=10 for wild-type mice. Statistically significant difference from control was calculated using Student t-test, P value ** <0.01, *** <0.001.

Figure 4

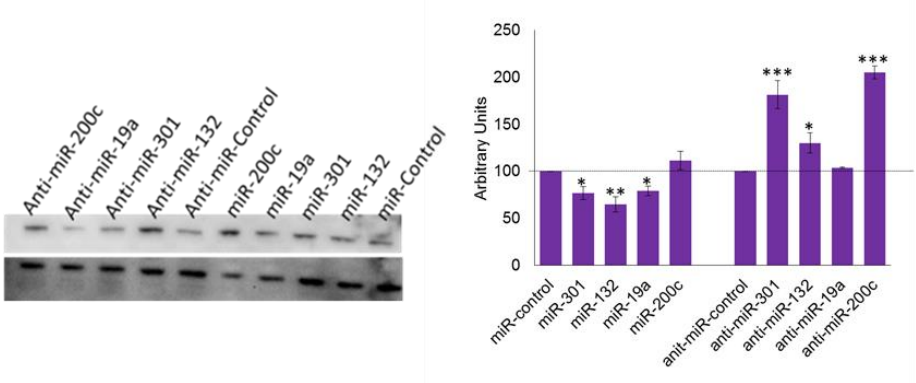

Figure 4 Western Blot analysis of Neuro2a cells transfected with miRNA or anti-miRNA 48 hours after transfection. Representative image shown (n=3). Statistically significant difference from control was calculated using Student's t-test, ** P value <0.01, *** P value <0.001.

Table1

miRNA	Fold Change	P Value
mir-547	-11.5	0.013
mir-872	-11.5	0.032
mir-150	-3.9	0.015
mir-27a	-3.3	0.050
mir-2138	-3.1	0.024
U87.A	-2.9	0.035
mir-27b	-2.4	0.009
mir-467F	-2.3	0.004
mir-106a	-2.0	0.024
let-7i	-2.0	0.025
mir-23b	-1.9	0.015
mir-152	-1.8	0.012
mir-411	-1.7	0.015
mir-30e	-1.7	0.025
mir-140	-1.7	0.008
mir-433	-1.5	0.049
snoRNA202.A	-1.2	0.007
mir-384-5p	1.4	0.043
mir-200c	556.6	0.027

Table 1 Significantly altered miRNAs in DRG from Mecp2 null mice. Mecp2 mRNA or protein is absent in homozygous null mice. Seventeen of the 19 miRNAs were downregulated (minus fold change). The largest observed difference was for mir-200c.

Table 2

Gene	Description	FPKM
miR-126	targets: bdnf, mmp16, ptger3, vegfa, scn7a, IL13	4165
miR-487b	targets: girk2, grm3	738.7
Ptger1	prostaglandin receptor e1	21.72
Alox12	arachidonate 12 lipoxygenase	11.59
Cxcr5	cytokine receptor	8.201
Pex14	peroxisomal membrane protein	3.81
Gpx1	glutathione peroxidate	3.428
Aif1	allograft inflammatory factor	1.713
Actb	beta-actin	0.007

Table 2 Genes and miRNAs identified from ChIP-seq. We initially identified ~ 100 genes with enriched MeCP2 binding in the DRG of SNI model mice compared to sham through comparative analysis and normalization to samples before immunoprecipitation. The genes shown in the table represent those selected for further studies based on their FPKM values and potential role in pain. FPKM represents the fragments per kilobase per million mapped and is a standard unit of ChIP-sequencing data.

Research Project 2: Project Title and Purpose

Making a Mouse to Study Hereditary Spastic Paraplegia – The purpose of this project is to generate and characterize a new transgenic mouse that expresses a human pathogenic mutant form of the SPG4 gene, which encodes for a protein called spastin. Mutations of this gene are the chief cause of Hereditary Spastic Paraplegia. The new mouse will be a key tool for studies on the etiology of the disease and the development of therapies for treating it.

Anticipated Duration of Project

1/1/2013 – 12/31/2014

Project Overview

Hereditary Spastic Paraplegia (HSP) is a debilitating constellation of neurodegenerative disorders that dramatically diminish the quality of life for patients. Mutations of *SPG4* are the most common cause, accounting for over 40% of HSP cases. *SPG4* codes for a protein called spastin, which is an enzyme that physiologically severs microtubules (MTs). Severing of MTs is important for mobility within the MT array of the axon, and for regulating MT number as well as the distribution of plus ends of MTs in the shaft of the axon and the synapse. In theory, too little or too much MT severing could be greatly detrimental to the vitality of the axon. Genetic analyses of the broad spectrum of mutations associated with *SPG4* have led to the predominate view that haploinsufficiency is the molecular mechanism of the disease. In this view, a reduction in the levels of active spastin results in MT severing insufficient to keep the adult axon vital. However, a haploinsufficiency model would not explain why the degeneration is specific to the corticospinal tracts, nor is it consistent with the lack of developmental disorders in the patients, as MT severing is particularly important for growing axons.

We propose a toxic gain-of-function model, in which axonal degeneration results not from inadequate MT severing but rather from toxic effects of the mutated spastin molecules that accumulate in the axons of afflicted neurons. Spastin has two start codons, and hence produces a full-length isoform called M1 and a slightly shorter isoform called M87. The shorter isoform is found throughout the nervous system during development and in the adult, but M1 is present in appreciable amounts only in the adult spinal cord. The hypothesis is that the mutant form of M1 is toxic and accumulates, while the mutant form of M87 is not so toxic and rapidly degrades. The goal of these studies is to generate a transgenic mouse expressing the M1 form of a pathogenic mutant form of human spastin, so that studies can be performed on the biochemical basis of its toxic properties and so that potential therapies can be tested.

Specific Aim 1. Generate a transgenic mouse model for *SPG4*-based HSP.
Specific Aim 2. Conduct behavioral analyses, focusing mainly on walking behavior.

Principal Investigator

Peter W. Baas, PhD
Professor
Drexel University College of Medicine
2900 Queen Lane
Philadelphia, PA 19129

Other Participating Researchers

Terry Heiman-Patterson, MD – employed by Drexel University College of Medicine

Expected Research Outcomes and Benefits

The expected outcome is the production of a new transgenic mouse that can be used as a model for Hereditary Spastic Paraplegia. This mouse will enable future studies on the mechanism of the

disease and allow potential therapies to be tested.

Summary of Research Completed

Aim 1 progress:
During this reporting period, we worked closely with a company to produce a new transgenic mouse that can be used as a model for Hereditary Spastic Paraplegia.

We decided to use the inducible Rosa26 model in which we introduce the human pathogenic mutant SPG4 (spastin) gene so that when the animals are crossed with different Cre mice, the protein is expressed in various different cell populations. We decided that rather than induce the expression of the M1 mutant exclusively, we would build the construct so that both mutant M87 and mutant M1 are expressed, as this would be closer to the human disease. According to our cell culture data, the mutant M87 should be relatively unstable and not accumulate, whereas the mutant M1 should be stable and accumulate. There are over 200 different mutations of SPG4 known to give rise to Hereditary Spastic Paraplegia, and we chose to use C448Y, as we understand it best from our recently published work on primary rodent neuronal culture and Drosophila (J. Neuroscience 34: 1856-1867). The mouse has been completed and has arrived at Drexel, where we are currently working to establish a colony and begin our efforts to cross the animals with Cre lines that will enable expression on CNS tissue. Our plan will be to perform initial behavioral studies but we are also prepared for potentially dramatic effects, given how toxic the mutant M1 can be, which may require recalibration and re-selection of other Cre lines before the behavioral studies can begin.

Research Project 3: Project Title and Purpose

Irreversible HIV-1 Inactivation for AIDS Intervention and Prevention – Agents have been discovered at Drexel University that can irreversibly inactivate HIV-1 before host cell encounter. These virucidal agents have the potential to prevent HIV-1 infection and spread by treatment at early stages of human exposure to the virus. In addition, viruses from already-infected individuals can be isolated, inactivated by these agents and then used as therapeutic vaccines in the infected donors. This project will examine the breadth of virucide action on different virus tropisms and subtypes, determine inactivation potency in cellular environments, determine the immunoreactivity of the inactivated virus and test the neutralization activity following inactivated virus immunization.

Duration of Project

1/1/2013 – 12/31/2013

Project Overview

The overarching goals of this project will be to establish the breadth and potency of irreversible inactivation of HIV-1 by an emerging class of envelope glycoprotein (Env) targeting inhibitors, and to determine how to use the intrinsic instability of HIV-1 Env as a basis to develop AIDS therapeutic vaccine and prevention strategies.

Inactivating HIV-1 before entry into host cells remains a compelling yet elusive means to prevent viral infection and spread leading to the AIDS pandemic. Host cell infection by HIV-1 is mediated by cell receptor interactions with trimeric envelope glycoprotein (Env) spikes that are exposed on the virus membrane surface. Env is the only virus-specific protein on the virion surface, and is essential for cell receptor interactions and subsequent virus-cell fusion. Hence, Env presents an obvious target to attack the virus directly in order to block the molecular recognition steps that lead to host cell infection. Env-specific inhibitors that could inactivate the virus before receptor encounter would hold great promise of inhibiting initial HIV-1 infection. Such inhibitors would provide virus-targeted molecular weapons to prevent AIDS transmission and disease progression, a global health priority. In spite of the great potential of Env targeting for AIDS prevention and therapy, progress has been limited. This CURE project will seek to fill this void with a recently revealed class of broadly active peptide triazole inhibitors that bind specifically and with high affinity to HIV-1 Env gp120, dual antagonize the interactions of Env with both host cell receptors CD4 and CCR5/CXCR4 co-receptor and, strikingly, cause envelope shedding and virus rupture leading to its complete inactivation before host cell encounter. Importantly, the residual inactive virion remains antigenically active, making it a potential attenuated vaccine. The properties of peptide triazole virucides make it feasible to use this type of agent as a microbicide to inactivate HIV-1 before virus uptake in mucosal tissues, and alternatively to produce inactivated virus particles for protective immunization.

Specific Aims:
Aim 1. Determine the breadth of inactivation potency of peptide triazoles against the major globally prevalent subtypes of HIV-1 and against infectious viruses from currently treated AIDS patients.
Aim 2. Evaluate the inactivation by peptide triazoles of viruses sequestered by dendritic cells and at the dendritic cell-T cell interface, virus reservoirs (including latently infected cells) and newly forming viruses from infected cells.
Aim 3. Define the antigenic properties of virus products obtained by peptide triazole inactivation through their gp120 shedding and virolytic rupture activities.
Aim 4. Measure immune responsiveness to inactivated virus products, including shed Env gp120 and residual virion Env gp41, in a small animal model.

Principal Investigator

Irwin M. Chaiken, PhD
Professor
Drexel University College of Medicine
11102 New College Building
245 N. 15th Street
Philadelphia PA 19102

Other Participating Researchers

Jeffrey Jacobson, MD; Michele Kutzler, PhD; Lauren Bailey; Rosemary Bastian; Andrew Holmes; Pamela Kubinski; Mariana Bernui, PhD; Pooja Jain, PhD – employed by Drexel University College of Medicine

Expected Research Outcomes and Benefits

This research project is based on discovery of a class of peptide triazoles that bind strongly and specifically to the envelope protein of the HIV-1 virus, are able to inactivate the virus by limited breakdown of its infectious structure and at the same time produce immunogenic products that could be used for protective immunization. The investigations will expand understanding of the process of virus inactivation and immunogenicity of virus breakdown products formed. The work seeks solutions for preventing and intervening with the spread of AIDS.

Summary of Research Completed

Background: AIDS pathogenesis is caused by HIV-1 cell infection mediated by trimeric envelope glycoprotein (Env) spikes on the exposed outer surface of the virus. Each Env trimer consists of two non-covalently associated glycoproteins, a gp41 transmembrane protein and an external gp120 surface protein and the interaction between HIV-1 envelope proteins and host cell receptors is critical for productive infection and thus a promising target for vaccines.

The production of gp41-targeted vaccines has been hindered by the inability of antibodies to bind to the most biologically relevant sites of the protein spike as they are conformationally hidden before binding. Therefore the identification of broadly neutralizing antibodies against epitopes on the highly conserved MPER region of the gp41 envelope protein makes this antigen a very attractive vaccine immunogen target. To date, immunization with whole protein forms of Env or its subunits have not elicited neutralizing antibodies; instead, non-protective epitopes dominate the immune response and divert the Ab response from protective epitopes. Thus, new approaches that target the production of Abs against conserved sites such as the MPER need to be developed. An MPER-based vaccine would direct Ab responses against this region, avoiding the problem of Abs against other sites on Env. Approaches to inhibit HIV-1 infection of cellular targets such dendritic cells and to inactivate latently infected cells once formed after infection also are needed.

Antigenicity of residual HIV-1 pseudovirus after peptide triazole thiol treatment (Aim 3)
Peptide triazole thiols, a class of dual-antagonist inhibitors (Dr. Chaiken's lab) target the spike gp120 protein and cause irreversible deactivation of the virus through shedding of the spike protein and leakage of the luminal p24 protein (Bastian et al, *Retrovirology* 2013). The gp41 subunit remains associated with the residual virus after gp120 shedding and p24 release, and this virion lacks an organized capsid. As shown in Figure 1 below, the overall lytic process was found not only to inactivate virus but also to expose a residual virion that is immunologically active in that the particles can be recognized by known monoclonal antibodies that bind to the membrane proximal external region (MPER) of gp41 (2F5, 4E10, 10E8 and Z13e1).

Purification of inactivated residual virions for immunization (Aim 4)
Inactivated virions derived from the peptide triazole thiol KR13 treatment of HIV-1 BaL.01were purified for use in mouse immunization experiments. The procedure used is depicted in Figure 2.

Murine immunization schedule (Aim 4)
Mice were immunized with KR13-derived residual inactivated BaL.01. The protocol used is shown in Figure 3.

Finding of immunogenicity as determined by serum content of MPER-binding antibodies (Aim 3)
Antisera collected from the immunized mice were tested for presence of anti-MPER antibodies. As shown in Figure 4, these were found with KR13-treated viruses in 3 of 6 mice so immunized, but in none of the mice immunized with the non-lytic KR13b, gp41 or formulation.

Preliminary finding of neutralizing activity in sera from mice immunized with KR13-produced residual virions (Aim 4)
As demonstrated in Figure 5, infection neutralization activity was detected in pooled sera from mice immunized with KR13-treated BaL virus.

Effects of KR-13 (or peptide triazoles, in general) in a model of HIV-1 latency (Aim 2)
Latently infected cells are those that contain integrated copies of the HIV-1 genome but do not express measurable amounts of viral proteins and do not produce progeny virions. These cells however pose a formidable barrier to HIV-1 eradication, since they are undetectable to the host's immune responses, and can serve as a source of new virions if viral protein and viral particle production is resumed, in a process called reactivation. To determine if peptide triazoles may have an effect in the context of reactivation from latent HIV-1 infection, the laboratory of Dr. Martin Garcia utilized latently-infected U1 monocytic cells, which contain transcriptionally-silent integrated pro-viruses that can be reactivated with various stimulatory signals, such as treatment with 100 ng/ml PMA. As expected, PMA resulted in virion production into culture supernatants, as detected by the presence of large amounts of the viral $p24^{gag}$ protein (quantitated using ELISA). In the absence of PMA, treatment with KR13 or AuNP-KR13 did not result in induction of $p24^{gag}$ in the culture supernatants, and when combined with PMA, they did not alter virion production and $p24^{gag}$ levels induced by PMA. Reactivated U1 cells produce CXCR4-using HIV-1_{IIIB} virions, and thus supernatants from U1 cells treated with PMA, KR13/PMA or AuNP-KR13/PMA were used as inoculum for HeLa-P4R5 cells, which are susceptible to infection by both CCR5- and CXCR4-using viruses, and produce beta-galactosidase in response to infection. Interestingly, we found that combination of PMA with KR13 or AuNP-KR13 led to a reduction in infectivity of the virion-containing supernatants, despite the similar $p24^{gag}$ levels. The reduction in infectivity was more pronounced with AuNP-KR13 than with KR13. This suggests that AuNP-KR-13, and KR-13 to a lesser extent, reduce the infectivity of newly produced virions by reactivated U1 cells.

Effect of peptide triazoles on dendritic cell infection (Aim 2)
Dr. Jain's laboratory conducted tests with the triazole derivative HNG-156, the peptide triazole thiol KR13, and the smaller peptide triazole analogue UM15 in both pre- and post-infection treatment models with B-THP-1 cells expressing DC-SIGN. For this, B-THP-1/DC-SIGN cells were infected with HIV-1_{BAL} pseudovirus, and the amount of total HIV-1 *gag* RNA was calculated as a measure for treatment response. First, DC-SIGN non-expressing cells (B-THP-1) contained lower viral RNA levels compared to B-THP-1/DC-SIGN cells, confirming importance of this receptor in HIV-1 binding and entry. Dextran (a polyglucoside), a known ligand of DC-SIGN and mannose receptor (CD206), was also tested in parallel as the control as well as in

combination with HNG. In each case, pre-treatment of cells with Dextran and/or virus with peptide triazoles provided significant protection to the infection. Some of these results were also validated in primary monocyte-derived dendritic cells.

Conclusions

In summary, both forms of peptide triazoles (KR13, KR13b/HNG156) inhibit viral infection as measured by infectivity (p24 release by infected cells). Treatment of virus with both forms of triazoles leads to shedding of gp120. KR13 treatment causes virolysis and leakage of p24. gp41 on KR13-treated residual viral particles are recognized by antibodies to MPER epitopes. Taken together our data suggest that delivery of peptide triazole-treated HIV-1 pseudoviral particle fractions to mice *in vivo* results in the development of antibody responses that will map to specific immunoreactive relevant MPER gp41 epitopes, and importantly, are able to generate functionally relevant neutralizing antibodies following immunization.

The novel method identified by our research team to generate a MPER-based immunogen could potentially be coupled with a novel in vivo electroporation-delivered DNA HIV-1 gag pol env vaccine arm in a prime boost strategy to elicit important protective immune responses.

Peptide triazoles showed some ability to prevent formation of infectious virus from U1 producer cell model of latently infected cells. Preliminary evidence was obtained suggesting that peptide triazoles can protect dendritic cells from HIV-1 infection. Hence, concerning cellular aspects, efforts through this research team also have identified possible approaches to use peptide triazoles to suppress early stages of infection at mucosal dendritic cell loci, and to suppress virus production from latently infected cells that could be important for patients with already established infection.

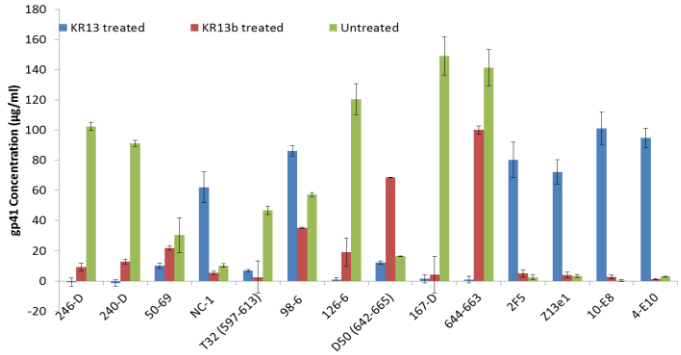

<u>Figure 1.</u> (A) Peptide triazole thiols (PT) target the spike gp120 protein and cause irreversible deactivation of the virus through shedding of the spike protein and leakage of the luminal p24 protein. (B) Antibody mapping studies depicting the gp41 epitopes exposed on the residual virion post KR13b (green bars, negative control peptide) treatment, KR13 treatment (blue bars) or untreated virion (red bars).

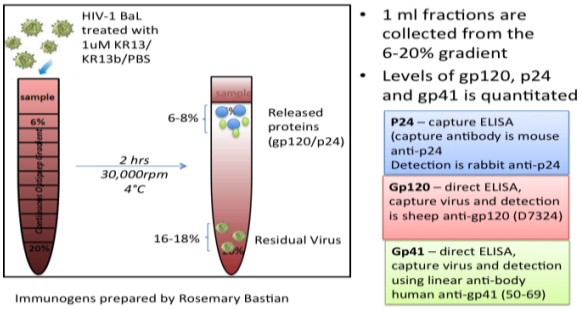

Figure 2. The HIV-1 BaL pseudovirions were treated for 30 min at 37°C with KR13, KR13b (1 µM) or PBS as negative control, and samples spun on a 6-20% iodixanol gradient. The residual virion in the 16-18% fractions will be pooled together. The residual virion post treatment will be fixed using equal volume of 0.1% paraformaldehyde and spun at 16,000 X g for 2 hours at 4°C in an Eppendorf table top centrifuge. The pellet is collected and ELISA was used to detect p24, gp120 and gp41 epitopes with human antibodies and followed by addition of anti-human IgG HRP (EMD Millipore) secondary antibody to quantitate immunogen.

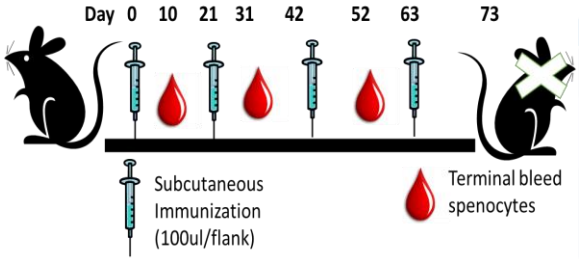

Group	Antigen	Dose
Formulation	Formulation (PBS/QuilA)	0ug
KR13 + HIV-1 Bal. 01	Formulation +KR13 HIV-1 Bal. 01	22ug gp41
KR13B + HIV-1 Bal. 01 (Negative control)	Formulation KR13B +HIV-1 Bal. 01	22ug gp41

Figure 3. Purified KR13-treated pseudoviruses were fixed with PFA and mixed 1:1 with QuilA adjuvant in sterile PBS, 100ul was injected subcutaneously into each flank for a total of 200ul/mouse. Ten days post final immunization, the animals will be sedated using an analgesic, and blood (sera) will be harvested and processed for immune analysis.

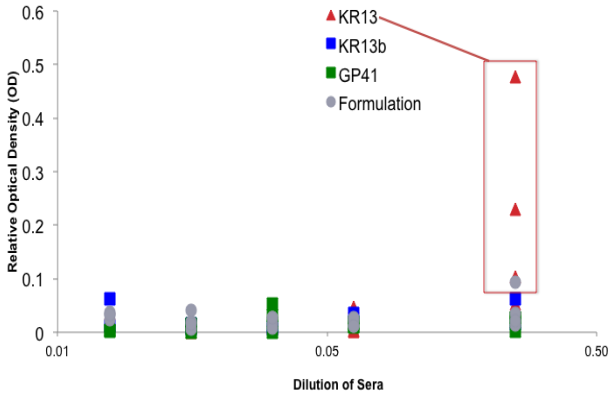

Figure 4. Ten days post final immunization, the animals were bled, and serum was processed for immune analysis. ELISA was carried out to detect mouse anti-HIV-1 MPER IgG (plates were coated with MPER peptides). Importantly, we observed high anti-MPER binding titers (O.D. 450nm) in 3/7 vaccinated mice to the KR13-treated virus (Panel B grey diamond symbols) following the last immunization.

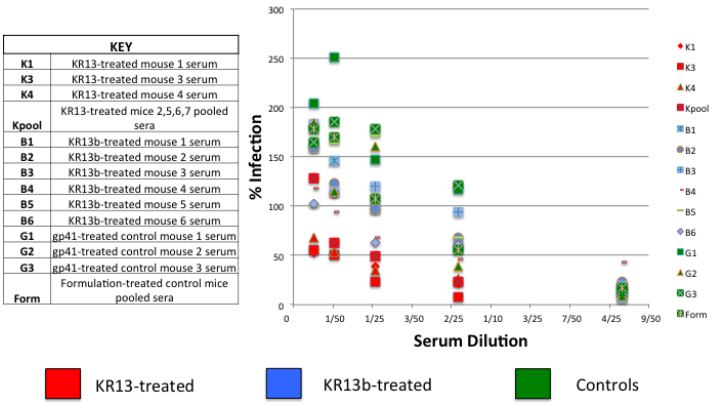

Figure 5. Ten days post final immunization, the animals were bled, and serum was processed for immune analysis. We verified that the antibody generated was able to compete for binding to gp41 in a conformational manner to the MPER region using a competition ELISA with 2F5 broadly neutralizing antibody specific to the highly conserved membrane-proximal external region (MPER). For the data shown above, sera were incubated at 56°C for 1 hour to destroy complement activity. After incubation, some sera were pooled to have enough for testing. Serum was serially diluted and combined with previously titered BaL.01 pseudovirus. The virus/serum solution is incubated 30 minutes at 37°C and then added to HOS.T4.R5 cells for infection. Media will be changed after 24 hours and the cells will incubate for an additional 24 hours. Cells were lysed with Passive Lysis Buffer (Promega) and multiple freeze-thaw cycles. The lysate was then used in a luciferase assay to determine %infection (neutralization).

Research Project 4: Project Title and Purpose

Phenotypic Diversity of Neurons Modulating Executive Function in ADHD – The purpose of this project is to examine the phenotypic relationship between the mammalian prefrontal cortex (PFC), the area of the brain responsible for executive function, and the locus coeruleus (LC), one of the major brainstem modulatory centers that regulate functional operations in the PFC, in both normal and ADHD rats. This research will inform the development of drugs that are potential treatments for attention disorders.

Duration of Project

1/1/2013 – 12/31/2013

Project Overview

The goal of this project is to examine the phenotypic relationship between the mammalian prefrontal cortex (PFC), the area of the brain responsible for executive function, and the locus coeruleus (LC), one of the major brainstem modulatory centers that regulate functional operations in the PFC, in both normal and ADHD rats. Our general hypothesis is that anterior cingulate cortex **(**ACC), mPFC and OFC are differentially regulated by subsets of LC neurons with distinct phenotypes and physiological properties in order to optimize executive function; and these neuronal phenotypes and physiological properties are altered or compromised in the SHR model of ADHD. There are four specific aims to test this intriguing hypothesis:

AIM 1: To determine the anatomical distribution and neurochemical identity of coeruleo-prefrontal cortical projection neurons.
AIM 2: To determine the molecular phenotype of LC neurons projecting to different cortical regions.
AIM 3: To determine the electrophysiological properties of LC neurons projecting to distinct cortical regions.
AIM 4: To evaluate the anatomical organization, molecular phenotype and physiological profile of LC projections to PFC in the spontaneously hypertensive rat (SHR) model of ADHD.

We expect to show how organizational features and physiological attributes of the LC-PFC projection promote adaptive behaviors and executive function in normal animals and how these features are altered in a well-accepted animal model of ADHD, i.e. the spontaneously hypertensive rat (SHR).

Principal Investigator

Wen-Jun Gao, PhD
Associate Professor
Drexel University College of Medicine
2900 Queen Lane
Philadelphia, PA 19129

Other Participating Researchers

Barry D. Waterhouse, PhD – employed by Drexel University College of Medicine

Expected Research Outcomes and Benefits

The goal of this project is to reveal phenotypic diversity (organizational, molecular, and physiological properties) of coeruleo-cortical projection neurons that impact specific executive behaviors in both normal and ADHD rats. The proposed studies will inform the development of drugs that are potential treatments for attention disorders. Moreover, this work will further validate the SHR model for use as a screen for ADHD therapies. The most important aspect of this project is the potential to demonstrate the functionally segregated populations of LC-prefrontal projection neurons. Although this is a basic science proposal, the results of the proposed studies would provide a framework for better understanding of genetically transmitted developmental disorders such as ADHD and new targets for development of novel therapies for ADHD and other neuropsychiatric disorders associated with noradrenergic dysfunction. If successful, similar approaches could be applied to transgenic models of schizophrenia, anxiety, PTSD, and depression.

Summary of Research Completed

AIM 1: Completed last report
AIM 2: Completed last report
AIM 3: Completed last report

AIM 4: Interestingly, we found that the LC neurons that project to PFC in the SHR rats exhibited variable spontaneous firing rates according to rat strain (Figures 1 and 2). As in the Spague-Dawley rat, LC neurons which project to mPFC are more spontaneously active in both SHR and WKY strains than those which project to M1. However, this difference was less pronounced in the SHR. This result may reflect more uniform levels of norepinephrine (NE) throughout prefrontal and motor circuitries during low tonic levels of LC output compared to the WKY and Sprague-Dawley. In addition, the evoked firing rates of LC-cortical projection neurons vary by rat strain and terminal field. Despite elevated basal firing rates of mPFC projection neurons in the SHR compared to M1 projection neurons, their firing frequencies in response to current injection did not differ (Figure 2). This is in contrast to cortical projection neurons from the WKY rat strain, whose responses to electrical activation more closely matched those we recently reported for the Sprague-Dawley rat in *Proceedings of the National Academy of Sciences* (Chandler, Gao & Waterhouse, 2014). This finding may suggest that during activation of LC, similar levels of NE are achieved across prefrontal and motor circuitries in the SHR, potentially uniformly impacting circuit properties of these areas and adversely affecting attentive behaviors. Furthermore, these data may have implications for the mechanism of the psychostimulant methylphenidate, which restores behavioral operations by preferentially inhibiting NE uptake in prefrontal cortical areas relative to other forebrain regions.

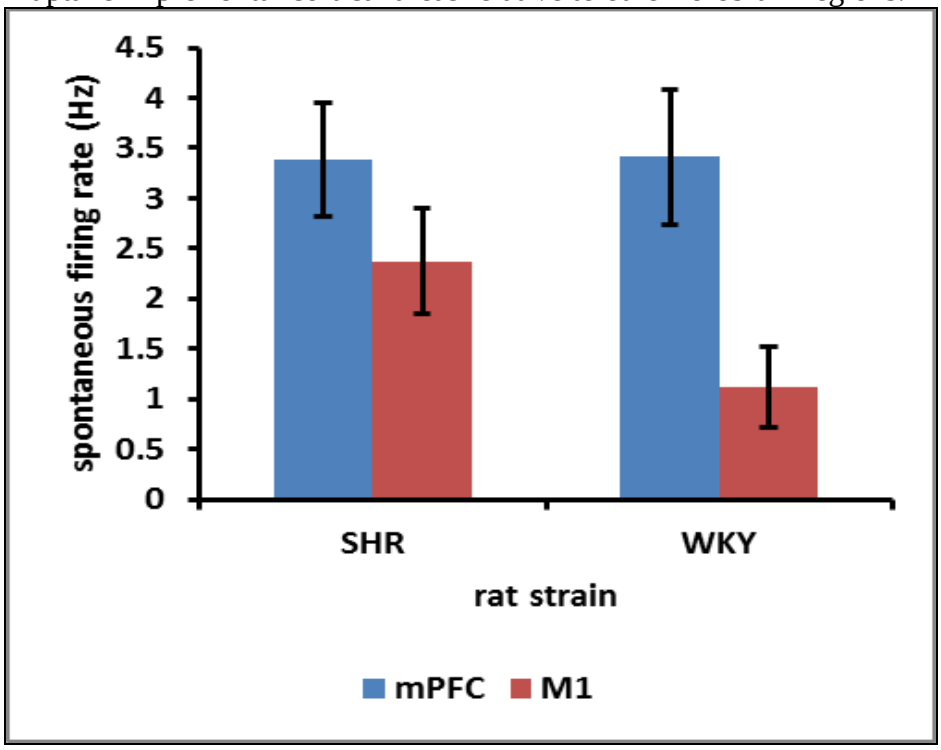

Figure 1. Spontaneous firing rates vary according to rat strain and LC-cortical terminal field. As in the Spague-Dawley rat, LC neurons which project to mPFC are more spontaneously active in both SHR and WKY strains than those which project to M1. However, this difference was less pronounced in the SHR.

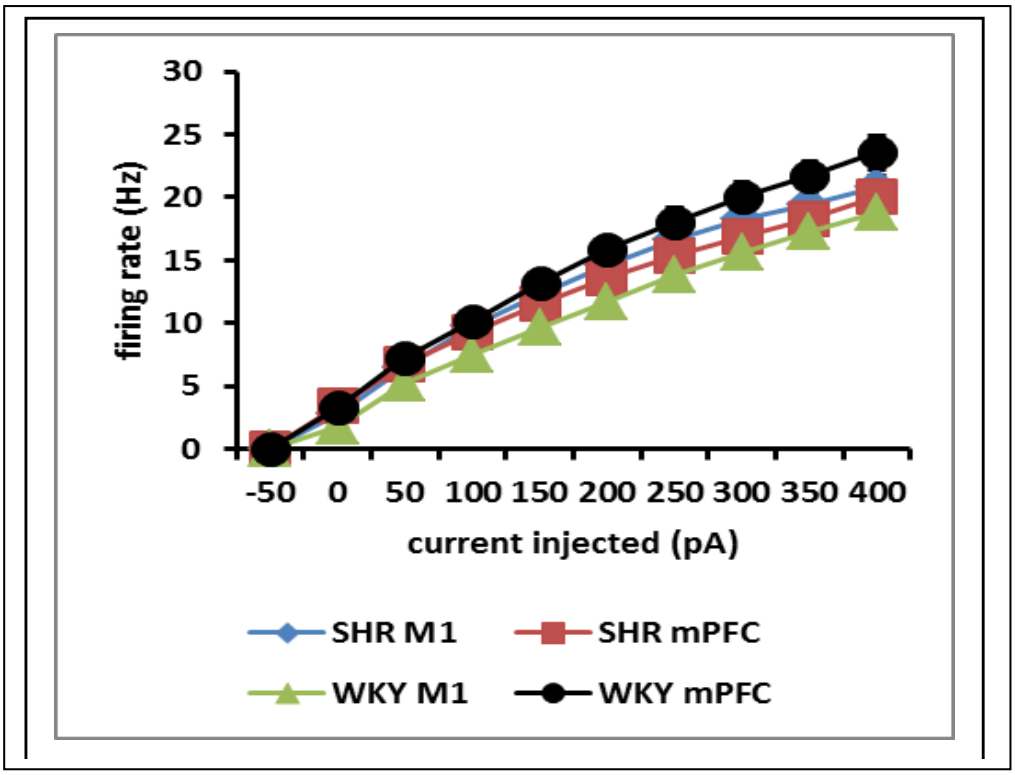

Figure 2. Evoked firing rates of LC-cortical projection neurons vary by rat strain and terminal field. Despite elevated basal firing rates of mPFC projection neurons in the SHR compared to M1 projection neurons, their firing frequencies in response to current injection did not differ.

Research Project 5: Project Title and Purpose

Investigating Nervous System Structure and Function by 2 Photon Laser Scanning Microscopy – A fundamental goal in neuroscience is to understand how neural circuits are formed and maintained in development, and throughout the life of the animal. Proper connectivity is critical to learning and memory processes in the healthy brain, and to functional recovery following injury or disease. Understanding the mechanisms regulating neural circuitry and connectivity is critical to developing therapies for treating neurological dysfunction as a result of injury or disease. This project aims to investigate the cell-cell interactions between astrocytes and dendritic spines, or synapses, in vivo. The results from this project will provide novel and important insight into the cellular and molecular mechanisms underlying astrocyte regulation of synaptic connectivity.

Anticipated Duration of Project

1/1/2013 – 12/31/2014

Project Overview

This project examines the role of astrocytes, the most abundant glial cell type in the CNS, in regulating the establishment and maintenance of dendritic spines during postnatal development, and in the mature brain. Spines are the principal sites of excitatory synapses, and serve as good indicators of synaptic function. In this project, we will use transgenic mice in which the molecular signaling pathway, Sonic hedgehog (Shh), has been targeted for disruption selectively in astrocytes. In Aim 1, we will examine whether Shh signaling in astrocytes is required for the development of dendrites and spines during early postnatal development. The morphological properties of dendrites and spines of Layer V neurons will be examined in the cortex at various stages during postnatal development, and in the adult brain. In Aim 2, we will use chronic, in vivo imaging by 2P LSM to examine the role of Shh signaling in astrocytes in the dynamic turnover of cortical spines. The rate of spine turnover will be examined in the cortex of adult mutants and controls to determine whether astrocytic Shh signaling is required for the structural reorganization of synapses. Together, these data will provide valuable insight into astrocyte-synapse interactions, and will facilitate future studies on the molecular and cellular mechanisms mediating synaptic plasticity.

Principal Investigator

Anna Denise R. Garcia, PhD
Assistant Professor of Biology
Drexel University
3245 Chestnut St., PISB 123.05
Philadelphia, PA 19104

Other Participating Researchers

None

Expected Research Outcomes and Benefits

This project aims to address the role of astrocytes in regulating the formation and maintenance of synapses *in vivo*. A more complete understanding of the mechanisms regulating neural circuitry and connectivity is critical to developing therapies for treating neurological disorders, and increasing evidence points to a critical role for astrocytes in establishing and maintaining neural circuits. In Aim 1, we will examine whether disruption of Shh signaling in astrocytes impairs cortical synaptogenesis during early postnatal development. If astrocytic Shh signaling is required for the establishment of normal synaptic connections in the cortex, then we expect to observe a concomitant disruption in the number and/or morphology of dendritic spines. In Aim 2, we will examine whether Shh signaling in astrocytes plays a role in the dynamic turnover of spines. If astrocytic Shh signaling is required for normal spine dynamics, then we expect to observe disturbances in the rate of spine addition and/or elimination following disruption of Shh signaling in astrocytes. The results from this project will provide new knowledge of how astrocytes contribute to the establishment of cortical circuits during postnatal development. Moreover, we will gain insight into the role of astrocytes in regulating the rearrangement of

synapses in the living brain. Taken together, these results will provide the foundation for further studies into the cellular and molecular mechanisms regulating astrocyte-synapse interactions, and will serve as preliminary data for future extramural grant support.

Summary of Research Completed

Progress on Specific Aim 1

Our previous data show that spine density of apical dendrites from Layer V neurons in the somatosensory cortex of adult GfapSmo CKO mutants (*GfapCre;Smo$^{fl/fl}$;Thy1GFPM*) is higher compared to controls (*Smo$^{fl/fl}$;Thy1GFPM*), whereas spine density at 2 weeks and 4 weeks of age is comparable between genotypes. GFP expression is developmentally regulated in Thy1GFPM mice, and at P7, the level of GFP expression is too low to detect a sufficient number of cells for high resolution morphological analysis of dendrites and spines. Moreover, our previous data showing similar spine densities at 2 and 4 weeks of age between mutants and controls suggests that early developmental spinogenesis is not dependent on astrocytic Shh signaling, and it is expected that similar results would be observed at time points earlier than 2 weeks. We have therefore focused our characterization at time points older than 4 weeks. We have performed further analysis of spine density from GfapSmo CKO mutants and controls at 6 weeks of age. Both GfapSmo CKO mice and controls show lower spine density at 6 weeks compared to 4 weeks of age, consistent with postnatal developmental pruning of synapses. Surprisingly however, GfapSmo CKO animals show a lower spine density compared with controls (Fig. 1). This suggests that at 6 weeks of age, the time at which synaptic pruning begins and cortical circuits are being refined, disruption of astrocytic Shh signaling impairs synaptic pruning processes, and further suggests that synapse pruning is accelerated in GfapSmo CKO mice. Alternatively, an increased rate of dendritic growth in GfapSmo CKO mice compared to controls could lead to a lower spine density. Further experiments using chronic, in vivo imaging of dendrites and spines are necessary to distinguish between these possibilities. Such experiments are currently being launched (see Aim 2).

Our previous study in the adult forebrain showed that distinct subpopulations of astrocytes express the transcription factor Gli1, indicating high levels of Shh signaling. Whereas ~35% of astrocytes in the cortex express Gli1, few astrocytes in the hippocampus are Gli1-positive, indicating that astrocytes in the hippocampus do not participate in Shh signaling. Previous studies have established a role for non-canonical Shh signaling within neurons in synapse formation between Layer II/III and Layer V cortical neurons. To rule out any non-specific effects of Smo deletion in neurons, we examined spine density of CA1 pyramidal cells in the hippocampus of GfapSmo CKO mice. Adult GfapSmo CKO mice and littermate controls were transcardially perfused with 4% PFA, cryosectioned at 40μm, and subsequently stained by brightfield immunohistochemistry for GFP. GFP-labeled pyramidal neurons in area CA1 of the hippocampus of mutants and controls were identified and traced by Neurolucida (MBF Biosciences). Indeed, spine density is comparable in pyramidal neurons in area CA1 of the hippocampus between mutants and controls (Fig. 2). This suggests that the increased spine density observed in the apical dendrites of GfapSmo CKO mutants is not due to a generalized effect on the transgenic animals, and supports the hypothesis that neuron-astrocyte communication through Shh signaling is required for establishing proper cortical circuitry.

To further rule out any non-specific effects of deleting Smo, and to support a specific role for astrocytic Shh signaling in establishing cortical circuits, we generated a conditional knock out of Smo in pyramidal neurons using a CamKinase2α Cre driver (*CK2αCre;Smo$^{fl/fl}$;Thy1GFPM*, referred to here as Ck2α Smo CKO). In contrast to GfapCre Smo CKO mice, CK2α Smo CKO mice show no signs of reactive gliosis. The number of cortical astrocytes expressing GFAP is comparable between CK2α Smo CKO mutants and littermate controls, and astrocytes in CK2α Smo CKO cortex show no signs of cellular hypertrophy. This is in contrast to our previous study in which we showed that targeted disruption of the obligatory Shh co-receptor Smo in astrocytes leads to increased GFAP expression in cortical astrocytes and hypertrophic cell bodies and processes. We examined the spine density of apical dendrites from Layer V cortical neurons in the somatosensory cortex of CK2α Smo CKO mutants and controls and observed no difference in spine density. This suggests that Smo-mediated Shh signaling in postnatal neurons is not required for spine development or long term maintenance, and further supports a specific role for astrocytic Shh signaling in regulating the synaptic architecture of Layer V cortical neurons. Taken together, these data support a role for Shh signaling in astrocytes in regulating the long term maintenance of cortical circuits. Aim 1 is complete.

Progress on Specific Aim 2

These funds were used to purchase a 2 photon laser scanning microscope (2P LSM) and necessary components and accessories, in order to enable multiphoton imaging. An Ultima In Vivo Laser Scanner microscope, and associated components, was purchased from Bruker Nano Surfaces. This microscope is equipped with 2 external non-descanned PMT detectors, as well as an Olympus Plan Achromat 10x/0.25 objective, and an Olympus Plan Achromat 40x/0.80 water immersion objective. To provide laser power to the microscope, a Chameleon Ultra II 3.5W Ti:Sapphire tunable laser was purchased from Coherent. The laser provides femtosecond pulses and can be tuned to 680nm – 1080nm, enabling multiphoton laser excitation of a broad range of fluorophores. The microscope and laser are situated on a 4' x 8' RS2000 Optical table with active leveling vibration isolators to isolate environmental vibrations and ensure high quality images, free of vibration-induced distortions. The 2P LSM is necessary to perform the experiments proposed in Aim 2. Moreover, the added capability for multiphoton imaging at Drexel University will greatly expand the research programs of existing faculty throughout the Drexel biomedical research community, and will facilitate novel collaborations throughout and beyond the University. In order to maximize the range of applications and users, the 2P LSM is also configured for *in vitro* slice imaging. Additional components of the multiphoton imaging facility include a dual channel perfusion heater controller, gas mixer, and culture dish incubation system, as well as a table top hood for preparing *in vitro* slices for imaging. The 2P LSM was installed in May 2014, and initial experiments investigating the role of astrocytic Shh signaling in the dynamic turnover of dendritic spines have now launched.

We have performed preliminary experiments in adult GfapCre Smo CKO mice and controls. A cranial window was implanted over the somatosensory cortex of *GfapCre;Smo$^{fl/fl}$;Thy1GFPM* mouse and a *Smo$^{fl/fl}$;Thy1GFPM* mouse. Animals were imaged over 2 days, following an 18 day recovery period. We analyzed the turnover ratio of spines from the apical dendrites of Layer V neurons within the first 100μm – 200μm from the surface of the brain. Turnover ratio was defined as the total number of spines that were added or eliminated/2x total number of spines

analyzed. The turnover ratio of GfapCre Smo CKO mice was lower than that observed in controls (CKO = 0.04, *n = 234* spines, Con 0.06, *n = 300* spines). This suggests that synapses are less dynamic in GfapCre Smo CKO mice than controls. We then analyzed the proportion of spines that were added or eliminated from each animal. Consistent with previous studies, spine elimination in the adult somatosensory cortex was greater than spine formation (Fig. 3). The proportion of spines that were eliminated over 2 days was comparable between mutants and controls (Fig. 3). In contrast, spine formation was lower in mutants compared to controls (Fig. 3). These data suggest that synaptic remodeling in the adult somatosensory cortex is reduced following disruption of Shh signaling in astrocytes, suggesting that neuron astrocyte communication through Shh signaling is required for normal synaptic plasticity. Experiments are currently underway to confirm these findings.

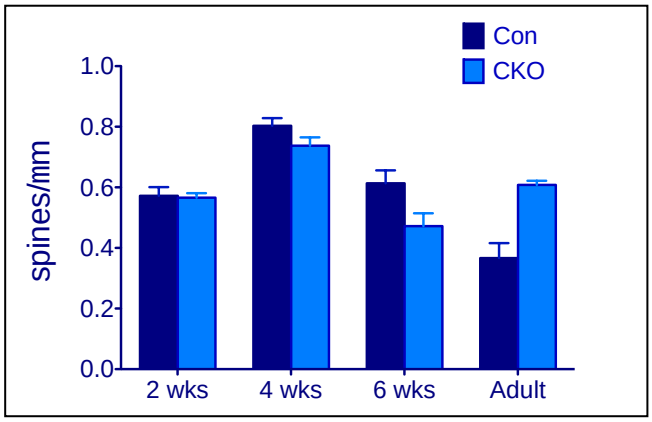

Figure 1. Spine density of apical dendrites from Layer 5 neurons from the somatosensory cortex of GfapSmo CKO mice and controls at 2, 4, 6 weeks of age and in adults.

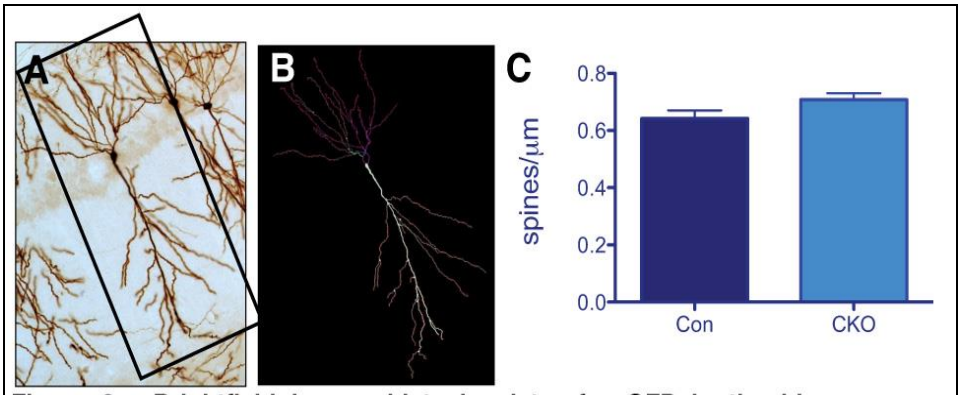

Figure 2. Brightfield immunohistochemistry for GFP in the hippocampus. (A-B) Immunohistochemistry for GFP (B) and Neurolucida tracing from pyramidal cell in area CA1 of the hippocampus of an adult GfapSmo CKO mouse. (C) Quantification of spine density of apical dendrites from CA1 pyramidal neurons.

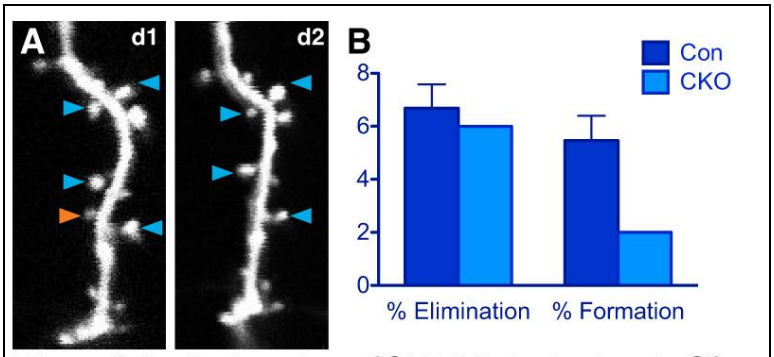

Figure 3. *In vivo* imaging of GFP-labeled spines in Gfap Smo CKO;Thy1 GFPM mice. (A) Repeated imaging of dendrites and spines from apical dendrites of Layer V neurons over 2 days. (►) Spines observed over both days of imaging. (►) Spine elimination. (B) Percentage of spines that were eliminated or formed over 2 days of imaging.

Research Project 6: Project Title and Purpose

Tumor Characterization in Breast Carcinoma Using Computerized Image Analysis – We have developed a computational method by which we can characterize lymph node metastasis status from histological images of primary breast tumor specimens. We propose to investigate the relationship between lymph node metastasis status and surrogate tumor markers, and to develop a novel machine learning technique designed to use histological images to predict tumor subtype, previously only possible with expensive molecular testing.

Anticipated Duration of Project

1/1/2013 – 12/31/2014

Project Overview

Histological methods have been shown to be a useful and cost-effective tool in determining pathologic stage. Regional lymph nodes status, primary tumor size, and distant metastasis are the three variables determining pathologic staging, as performed routinely for clinical cancer. Additionally, the Nottingham Prognostic Index utilizes tumor size, histologic grade, and lymph node status to stratify patients and determine appropriate treatments. However, the main disadvantage of grading is its lack of consistency, which can only provide moderate reproducibility in some studies, and which can be affected by the experience of the pathologist issuing the pathology report. We have developed an automated procedure to objectively determine metastasis status via computerized image analysis of primary breast tumor histology. The generalizability of this procedure to other factors determining tumor status and sensitivity to therapeutic interventions has yet to be examined. The successful development of a reliable algorithm based on histological image analysis can potentially supplant molecular tools for the characterization of tumor subtypes and therapeutic strategies in breast carcinoma patients.

Specific Aim 1: To evaluate the predictive success of computerized histological image analysis using surrogate tumor markers. We will generate predictions of metastasis status from histopathological images of primary breast tumor specimens, and compare these predictions to immunohistochemical data commonly used to describe tumor aggressiveness and sensitivity. Our preliminary results indicate a strong correlation between predicted metastasis status and Ki-67, a measure of proliferation. We hypothesize that our image analysis paradigm provides information that can predict tumor status and guide treatment.

Specific Aim 2: To predict tumor subtypes via computerized image analysis of primary breast tumor histology. It has been shown that molecular diagnostic tools have a high degree of success determining tumor status and patient outcomes. We will develop an image analysis paradigm to use mRNA-defined tumor subtypes to train a multi-class machine learning classifier. We hypothesize that tumor subtypes can be predicted from histopathological image features, providing a cost-effective tool to define therapeutic groups.

Principal Investigator

Fernando U. Garcia, MD
Professor
Drexel University College of Medicine
245 N. 15th Street
Philadelphia, PA 19102

Other Participating Researchers

David E. Breen, PhD – employed by Drexel University
Mark D. Zarella, PhD – employed by Drexel University College of Medicine

Expected Research Outcomes and Benefits

Breast cancer (BCa) is a very common carcinoma that affects 1,300,000 patients worldwide and is responsible for 450,000 deaths every year. BCa is a heterogeneous disease encompassing multiple morphologies and different outcomes. Most invasive mammary cancers are classified as invasive ductal carcinoma not otherwise specified (IDC NOS), whereas about 25% are defined as histological "special types". These special-type BCas are categorized into at least 17 discrete pathological entities. Current therapy decision-making is increasingly governed by the molecular classification of breast cancer. Currently, BCas are subclassified by global gene expression profiling into 4 major subtypes that inform therapy decision making: luminal A, luminal B, HER2-overexpressing and basal-like (triple negative). Recently, the Cancer Genome Atlas Network described how the phenotypic variation between BCa occurs within, but not across, these major subtypes, highlighting the importance of identifying each BCa for appropriate therapeutic decisions. Currently, there are two ways to characterize BCa into these subtypes: 1) Utilizing the gene expression profile and 2) Utilizing immunohistochemistry (IHC) for the estrogen receptor (ER), progesterone receptor (PR), proliferation marker Ki-67, and human epidermal growth factor receptor-2 (HER2) as surrogate markers. Both of these solutions are costly and unsuitable for underdeveloped countries. We propose to develop an economical and

reliable alternative that can classify specimens into these subtypes in order to provide adequate treatment to patients from rural and underserved areas in Pennsylvania.

Summary of Research Completed

Aim 1

Data collection

This project relies on an analysis of imaging data obtained from the department's clinical activities. The imaging data is coupled in a deidentified fashion to a set of demographic, histological, and clinical information that allow us to select cases that meet specified criteria (e.g., patients that have not previously received chemotherapy, carry a diagnosis of invasive breast carcinoma, are not male). Since the start of the grant, we have been incorporating new cases into the database and assuring that the information is complete and accurate by reviewing the pathology reports. In our previous progress report, we identified 356 candidate cases for inclusion into the study. Many of those cases were excluded from the study due to clinical variables that did not meet the criteria we specified in the grant proposal. At present, with the assistance of a medical student summer research fellow, our current database includes 400 cases.

Importantly, for cases that exhibited Her2 staining considered equivocal by the College of American Pathologists (CAP), we obtained Fluorescence in situ hybridization (FISH) data to determine Her2 positivity in accordance with CAP guidelines, and incorporated it into the database. As a result, our database no longer excludes Her2 equivocal cases, which may previously have been a source of bias.

Subtype characterization from immunohistochemistry data

The segregation of cases into one of four breast subtypes is a critical step in the project. As we described in our proposal, using ER/PR and Ki-67 percent positivity along with Her2 staining intensity serves as a surrogate for gene expression analysis, and exhibits a fair degree of concordance. A recommendation was provided in a report published in 2011 detailing the staining properties that can be used for subtype categorization. During the latest reporting period, however, a refined method was published that demonstrated that PR status and a new Ki-67 threshold more accurately segregated Luminal B from Luminal A tumors. Additionally, this paper demonstrated that Her2-positive cases that are ER-positive belong to the Her2-amplified subtype, whereas previously they were considered Luminal B tumors. We incorporated these very significant changes into our ground truth definition to retrain our classifiers. Furthermore, recent CAP recommendations altered the thresholds for determining Her2 positivity. We also incorporated these changes into our ground truth definition.

Subtype definition using nuclear morphometry

The first specific aim of the project is to construct a classifier to use tumor architecture and nuclear morphometry to predict tumor subtype defined by immunohistochemistry. This is considered a *supervised* machine learning approach, as it uses immunohistochemistry data to define the ground truth (tumor subtype), which is then used to build classifiers in a way that minimizes prediction error. To demonstrate that there is inherent information in the images that can potentially be harnessed to build these classifiers, we first employed an *unsupervised*

procedure. This procedure identifies natural subdivisions in the nuclear morphometric characteristics of our cohort using hierarchical clustering. We applied morphological operations to segmented images, as described in the proposal, and generated a single value per case that represented its shape characteristics in a multidimensional space. We used the values for 147 ER-positive cases to construct a dendrogram to depict the groupings of cases with similar nuclear shape characteristics. We related the dendrogram to the staining properties of these cases and discovered that many clusters correspond to specific staining properties; for example, high Ki-67 and Luminal A characterization, as shown in Figure 1. This result confirms that nuclear morphometry contains information that can be harnessed to predict tumor subtype in ER positive tumors. We believe that such maps can also be used to visually compare the result of alternate subtype definitions, which will assist in comparing the results from Specific Aims 1 and 2. This result was presented at the 2014 USCAP conference.

A decision tree-based machine learning strategy for subtype characterization

In order to build a classifier to categorize breast tumors into one of four subtypes, it is necessary to develop a machine learning method that accurately categorizes multidimensional data into more than two groups. Previously, we used support vector machine (SVM) learning to predict whether a breast tumor had spread to the axillary lymph nodes. This procedure partitioned the data space into two regions by constructing a hyperplane that optimally divided the multidimensional training data. Subtype categorization introduces added complexity because the number of possible solutions is four (Luminal A, Luminal B, Her2-amplified, Triple negative) rather than two (metastasis, no metastasis). SVM currently does not support multi-class learning.

We developed and implemented a novel strategy that places multiple SVM classifiers in a decision tree framework. Figure 2A depicts a schematic of this strategy. We applied this technique and, after weighting each nuclear feature by an experimentally derived value (Figure 2B), we show a correct rate of 66.7% for ER status prediction for the 90 cases that we tested. This result was presented at the 2013 Drexel Discovery Day.

Nuclear segmentation of H&E images

The nuclear metrics we use as shape descriptors in our algorithm rely on an accurate identification and demarcation of cell nucleus contours. In our previous progress report, we hypothesized that texture gradients computed within isolated feature domains could serve as the substrate for segmenting cell nuclei. We have experimented with two additional methods by which cell nuclei can be segmented in histological images; we have successfully implemented one method in ER stained images. The shortcoming with this approach, however, is that it relies on stained nuclei, and cannot therefore be applied to ER-negative cases. The second method, which is still under development, can be applied to H&E images and therefore can segment all nuclei in our entire cohort. Both methods are described below. A graduate student in the lab who was funded by this project in 2013 worked on the nuclear segmentation component of this project and presented some of these results at the 2013 Drexel Discovery Day.

Segmentation of ER stained images was accomplished by first classifying all pixels in the image as either stained or unstained. SVM was used to perform this classification after being trained by manually identified nuclei. We found that Watershed segmentation, when applied to the classified images, tended to oversegment the nuclei; that is, it overestimated the number of nuclei

in the image by generating contours within single nuclei. We developed a safeguard against oversegmentation by discarding contours generated from "shallow" Watershed basins using an experimentally derived threshold.

Given the relatively complex color properties of H&E stained images, we are developing an alternative method for nuclear segmentation by identifying contours from gradients in an optimized H&E color space. We have successfully used machine learning to classify pixels in H&E images as belonging to a particular structure (e.g. stroma, nuclei, cytoplasm, lumen). Importantly, the confidence of the classification of each pixel is estimated by measuring its projection on an experimentally derived vector in hue-saturation-value (HSV) space. This vector represents the combination of hue, saturation, and value that optimally separates the structure from other pixels in the image (Figure 3). As a result, each pixel is assigned a scalar value that can be used as the "front end" for a gradient-based segmentation algorithm. By producing an accurate segmentation routine tailored to H&E images, we will be able to accurately identify cell nuclei independently of the hormone receptor and proliferative marker status of the tumor.

Aim 2: No progress was made during this period.

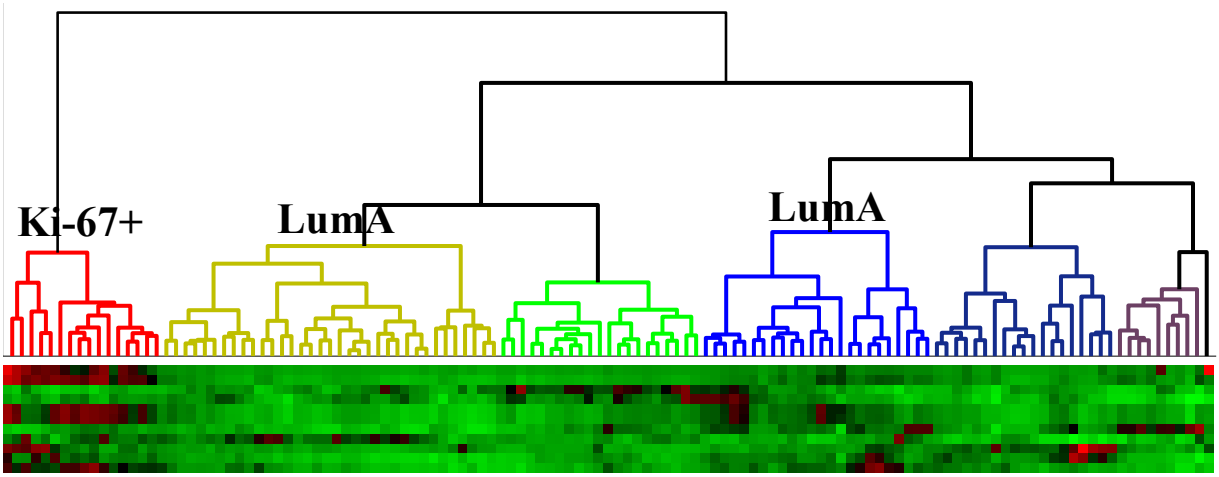

Figure 1. The heat map shown at the bottom represents the mean nuclear shape value for each of eleven shape metrics, normalized by each metric's mean and standard deviation. Each column represents a single case. The dendrogram above depicts the grouping of cases according to similarity in their shape characteristics. The height of the connecting line between any two cases represents the Euclidean distance between them.

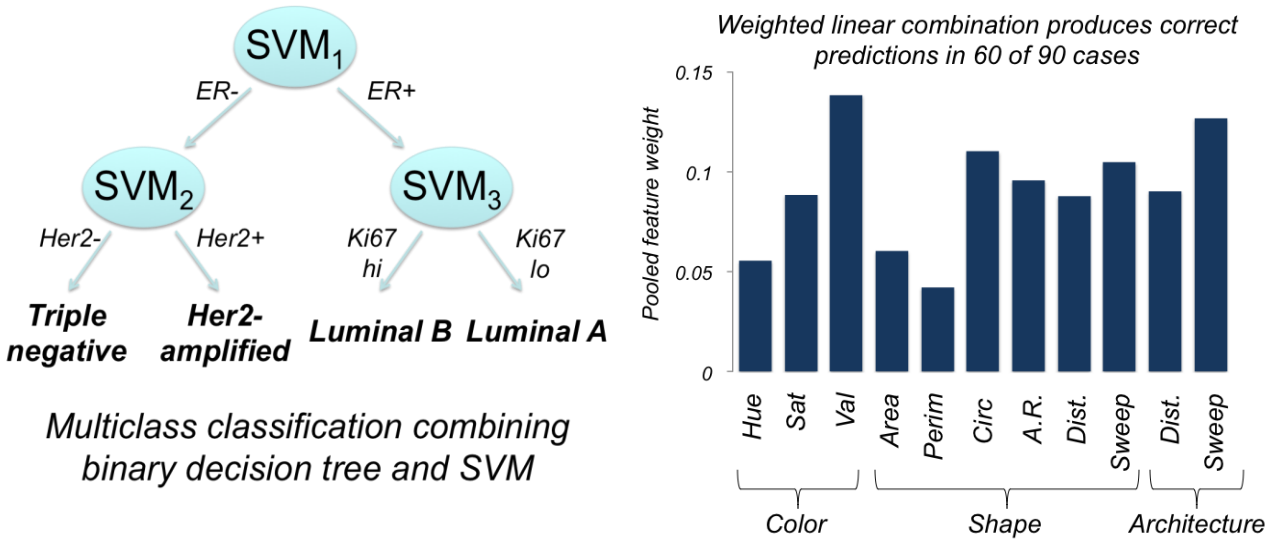

Figure 2. (A) A decision tree specified the order of classifiers (denoted SVM) to apply to each case. The outcome of SVM_1 defines whether to apply SVM_2 or SVM_3 next. Classifiers were trained with data sets defined by immunohistochemistry staining properties. Cases were partitioned into ER+ and ER- groups to train SVM_1, Her2+ and Her2- groups to train SVM_2, and Ki-67+ and Ki-67- groups to train SVM_3. (B) By applying an additional machine learning stage that iteratively optimized a set of weights for each feature, the prediction sets formed for individual features after applying SVM_1 were weighted and summed to produce scores that predicted ER status. The weights are shown above, and demonstrate that features from all three feature classes contributed to ER status prediction.

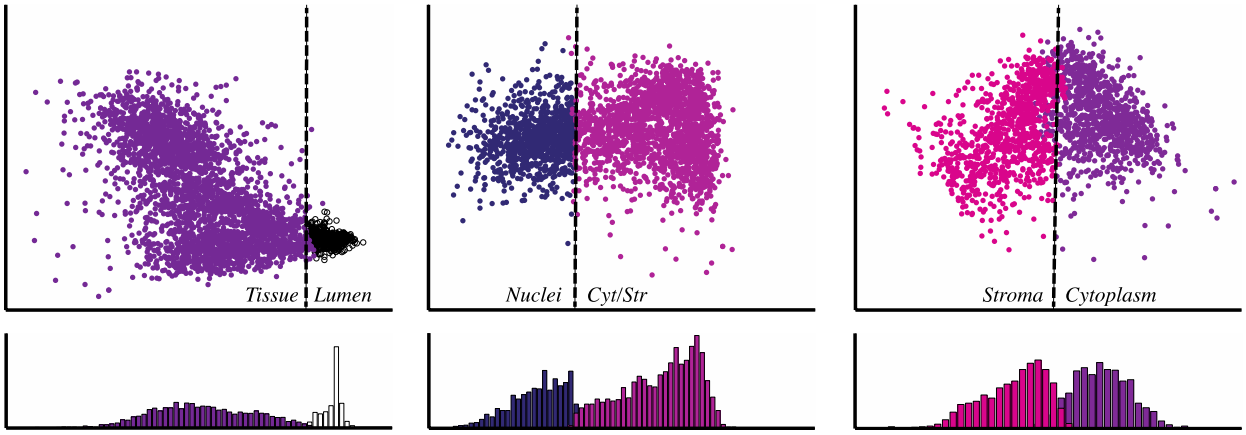

Figure 3. Each scatter plot shows the HSV values (projected to 2D) of pixels categorized by a user in a single H&E stained image. 2D projections were determined by first finding the optimal plane in HSV space that separated the two categories under study, and rotating the space in a direction normal to the plane. The plane is depicted with the dashed line. Projections onto the horizontal axis are shown in the histograms at the bottom. (Left) Tissue (nuclei, cytoplasm, stroma) vs. lumen. (Center) Nuclei vs. cytoplasm, stroma. (Right) stroma vs. cytoplasm.

Research Project 7: Project Title and Purpose

Innate Immunity and Bacterial Pathogenesis – The project aims to understand how innate immunity during viral-bacterial co-infections regulates susceptibility and pathogenicity and to establish models that allow the determination of important innate pathways that control infection. The studies proposed in this project will investigate important aspects of innate immunity in the context of bacterial infections. These studies will establish important models to understand the complex interaction between *N. gonorrhoeae* and HIV, and elucidate host factors that contribute to resistance to *L. pneumophila*.

Anticipated Duration of Project

1/1/2013 – 12/31/2014

Project Overview

The foci of this project are to understand how innate immunity during viral-bacterial co-infections regulates susceptibility and pathogenicity and to establish models that allow the determination of important innate pathways that control infection.

AIM 1: Determine the effect of bacterial and viral co-infection on epithelial innate immune responses and susceptibility to infection. Using an in vitro cervical epithelial cell model of *N. gonorrhoeae* and HIV-1 co-infection, we will investigate inflammasome-mediated innate immune responses that impact pathogen transmission.

AIM 2: Establish a model to identify critical innate responses that protect from L. pneumophila. A. Identify the innate immune response components that are triggered by *L. pneumophila* in human macrophages. B. Using influenza virus infection of mice, which induces innate immune paralysis and increases susceptibility to secondary bacterial infections, we will determine the critical innate factors that confer resistance to *L. pneumophila.*

AIM 3: Determine whether innate immunity triggered by acALY18, an endogenous peptide activator of inflammasomes, can inhibit infection or enhance control of N. gonorrhoeae and L. pneumophila.

Principal Investigator

Shira Ninio, PhD
Assistant Professor
Drexel University College of Medicine
2900 Queen Lane
Suite G47A
Philadelphia, PA 19129

Other Participating Researchers

Peter Katsikis, MD, PhD; Carol Artlett, PhD; Fred Krebs, PhD; Richard Rest, PhD; Yvonne Mueller, PhD; Sandhya Kortagere, PhD; Sihem Sassi-Gaha; Courtney Marin – employed by Drexel University

Expected Research Outcomes and Benefits

Co-infections are becoming increasingly important with the spread of antibiotic resistance and the potential for co-infections with other classes of pathogen such as viruses. The innate immune response is a key process in determining host resistance or susceptibility to infection and regulates the initial host response to microbes. These responses will either prevent, control, or eliminate the infection. Not surprisingly, some pathogens have evolved strategies to evade detection by, or inhibit innate immunity by interfering with the detection system of the host. Indeed, it has been found that many of these evasion strategies are crucial for the virulence of the pathogen. Additionally, inhibitory or activating effects of a pathogen on the innate immune system can alter the susceptibility of the host to a different pathogen aiding in co-infections. Infection with one pathogen, by triggering or inhibiting the innate response can create a host environment that facilitates or promotes the co-infection with a different pathogen. With these studies, we expect to understand the host factors and interactions that control resistance and susceptibility to bacterial pathogens. In addition, these studies will establish important models to understand the complex interaction between *Neisseria gonorrhoeae* and HIV, and elucidate host factors that contribute to resistance to *Legionella pneumophila*. Additionally, these studies will investigate the therapeutic potential of an inflammasome activator that has been shown to clear pathogen in simple infection models that will be tested in these novel models of complex infections.

Summary of Research Completed

Aim1 Progress: These studies were made possible through our prior expertise (Krebs) in the use of a transwell model of the cervicovaginal epithelium. This model system, which replicates the polarized topology of the female reproductive tract (FRT), provides the opportunity to introduce sexually transmitted pathogens to the apical (outer) side of the epithelium and monitor resulting innate immune responses on the basolateral (inner) side of the epithelial layer, as well as changes in the barrier created by the polarized epithelial cells.

As a prelude to understanding the combined effects of the human immunodeficiency virus type 1 (HIV-1) and *N. gonorrhoeae* in this model system, the initial experiment was designed to investigate the effects of *N. gonorrhoeae* infection alone, and to establish baseline measurements for subsequent experiments in which HIV-1 and *N. gonorrhoeae* would be introduced concurrently. In these studies, immortalized human ectocervical cells (Ect1/E6E7) were plated in transwell tissue culture inserts at a density of $1.5x10^5$ cells per well in serum-free media. The transwell tissue culture system includes an insert with a semi-permeable membrane (0.4 μm pore size) on which cells are grown. In this model of the cervicovaginal epithelium, the cells were maintained in the upper chamber in the presence of a cervicovaginal fluid simulant (CFS), which approximates the chemical content of cervicovaginal fluid that bathes the apical side of the

epithelium *in vivo*. The transwell insert is placed in a receiver plate (24-well format) containing media that comprises the lower chamber of the culture system. Cells were maintained for a period of approximately 16 days to permit cell growth into a confluent monolayer and the establishment of intercellular tight junctions. Cell confluence was monitored visually, while tight junction integrity was tracked by measuring trans-epithelial electrical resistance (TEER) between the upper and lower chambers. The epithelial barrier was considered established when TEER values had plateaued for at least three consecutive days. *N. gonorrhoeae* (strain FA1090) used for this experiment was cultured in overnight in GC Broth II and diluted to 0.3 OD_{600}, which yields a cell density of approximately $4x10^6$ colony forming units (CFU) per ml.

Semen samples used in these studies were obtained commercially (Lee Biosolutions, Inc.) from anonymous healthy donors. Samples from six donors were pooled to produce a sample volume representative of an "average" male. Whole semen was diluted to 25% (by volume) in these studies to mimic the degree of semen dilution that takes place during and after coitus.

Once the Ect1 cells had reached a TEER plateau, the CFS in each upper well was removed and replaced with approximately $4x10^4$ CFUs of *N. gonorrhoeae* suspended in CFS. Alternatively, a mixture of *N. gonorrhoeae* and whole semen (25%) in CFS was applied apically to the epithelial cells to simulate the simultaneous introduction of *N. gonorrhoeae* and semen during intercourse. EDTA, which causes a breakdown of tight junctions through chelation of divalent metal ions, was used as a positive control for reductions in epithelial barrier integrity. After incubation for 4 hours at 37°C, cells in the upper chamber were washed extensively and supplied with new media. Media in the basolateral (lower) chambers was collected for cytokine analysis, then replenished. TEER for each well was measured at 5-minute intervals from initial exposure (time = 0) through 30 minutes post-exposure, and at 1, 2, 3, and 4 hours post-exposure. At 24 hours post-exposure, media samples were again collected from the lower chambers for future analysis. Cells were also evaluated subjectively throughout the experiment for reductions in cell numbers associated with *N. gonorrhoeae* exposure. Prior experiments have demonstrated that a 4-hour exposure to 25% seminal fluid causes negligible reductions in cell viability. Basolateral conditioned media samples from 4 hours post-exposure were analyzed using the Human TLR-induced Cytokines II: Microbial-induced Multi-Analyte ELISArray Kit (Qiagen), which assays the following cytokines and chemokines: TNFα, IL-1β, IL-6, IL-12, IL-17A, IL-8, MCP-1, RANTES, MIP-1α, MIP-1β, MDC, and eotaxin.

Measurements of TEER indicated rapid and profound reductions in epithelial barrier integrity during the 4-hour exposure period (Fig. 1). As expected, addition of EDTA to the upper chamber caused a rapid and persistent decrease in TEER to 10% of resistance levels measured across in mock-exposed cells. While addition of *N. gonorrhoeae* also resulted in a rapid and considerable reduction in TEER (~50% at 5 minutes post-exposure), the reduction was less than that produced by EDTA, with TEER reaching a plateau of approximately 40%-50% during the first 30 minutes of exposure. After 30 minutes post-exposure, there was a second decline in TEER, reaching approximately 10% at 4 hours after the introduction of *N. gonorrhoeae*. Although small changes in cell morphology were evident in cells exposed to *N. gonorrhoeae* alone (and less so in cells exposed to *N. gonorrhoeae* and seminal fluid), exposed cells at 24 hours post-exposure were indistinguishable from mock-exposed cells, suggesting no gross reductions in cell viability or confluence.

In contrast, reductions in TEER in the presence of both *N. gonorrhoeae* and seminal fluid were much less relative to *N. gonorrhoeae* or EDTA exposure. After TEER values dropped to approximately 70% in the first 10 minutes, they increased steadily to approximately mock levels by 1 hour and declined again to ~70% by 4 hours post-exposure. The lesser effect of *N. gonorrhoeae* on TEER in the presence of seminal fluid is consistent with our previous demonstration that seminal fluid exposure results in considerable and rapid increases in tight junction integrity (TEER) over this same time period. The current results suggest that seminal fluid is able to partially abrogate the losses in tight junction integrity mediated by the presence of *N. gonorrhoeae*.

TLR-induced cytokines and chemokines accumulated in the basolateral chamber were analyzed with respect to levels found in mock-exposed cells. The response after exposure to either *N. gonorrhoeae* or *N. gonorrhoeae* and seminal fluid was dominated by the increased release of IL-8 (Fig. 2). The amount of IL-8 released from cells exposed to *N. gonorrhoeae* combined with seminal fluid appeared to be greater than the amount released from cells exposed to *N. gonorrhoeae* alone (~3.0- and 2.3-fold, respectively), suggesting an additive effect on IL-8 release. This finding is consistent with increased inflammation subsequent to epithelial seminal fluid exposure noted in our experiments and by other groups. Macrophage-derived chemokine (MDC) was also slightly elevated, particularly after cell exposure to both *N. gonorrhoeae* and seminal fluid. Notably, the concentrations of some soluble factors were reduced after exposure, including IL-6, IL-12, IL-17A, MCP-1, and eotaxin. With the exception of IL-6, factor concentrations were reduced similarly by *N. gonorrhoeae* alone or *N. gonorrhoeae* and seminal fluid.

Results of these studies indicate that the presence of *N. gonorrhoeae* in the FRT has an adverse effect on the integrity of the ectocervical epithelial barrier. However, the presence of seminal fluid during *N. gonorrhoeae* transmission may be protective through the abrogation of this effect. Furthermore, the results of the cytokine analyses indicate a multi-factorial innate immune system response mediated by the ectocervical epithelial cells. Although the response to *N. gonorrhoeae* and seminal fluid is dominated by an additive pro-inflammatory IL-8 release, there are also reductions in other factors that contribute to the overall immune response.

Aim 2 Progress: Using an experimental system we established in the previous reporting period we set out to test the effect of FlaA expression on the ability of human cells to restrict *L. pneumophila* replication. For this purpose we used de-identified human monocytes from healthy blood donors. The cells were obtained from the University of Pennsylvania's Human Immunology Core (operating under the supervision of the University of Pennsylvania's Institutional Review Board). Cells were differentiated into macrophages *in vitro* using recombinant human-MCSF, over the course of 7-8 days. Differentiated macrophages were then infected with various strains of *L. pneumophila* at a multiplicity of infection of approximately one bacterium per cell. Cell monolayers in 24-well dishes were infected with 2.5 x10^5 *Legionella* isolated from 2-day-old plate-grown cells. After 2 hours of infection, each well was washed with PBS three times and then 1 ml of fresh media was added. 72 hours post infection supernatant from each well was collected and then the monolayer was lysed with sterile dH2O. Bacteria were collected, serial diluted, and three dilutions were plated on CYE agar. After 3 days of incubation at 37°C, colony forming units (cfu) were counted to calculate bacterial cells per milliliter. The strains tested were all derived from *L. pneumophila* strain LP01 that was isolated from the

historic 1976 *Legionella* outbreak in Philadelphia. As a control, we used a wild-type strain LP01 and compared its growth to the isogenic strain LP01 *dotA* that lacks a functional type IVB secretion system and therefore is unable to replicate inside eukaryotic cells. As expected from our previous results, human macrophages support robust replication of *L. pneumophila*, and replication occurs in a mechanism that requires an intact type IVB secretion system (Fig.3). To determine if human macrophages have the ability to restrict *L. pneumophila* growth by detecting the flagellar protein FlaA, we compared wild type strain JR32 and an isogenic mutant JR32 *flaA*. Our results show that the mutant lacking the *flaA* gene, was able to replicate to a greater extent within human cells, compared to the isogenic wild type strain JR32 (Fig.3). These results suggest that human macrophages have an innate ability to detect and react to the *legionella* FlaA protein, and perhaps to similar flagellar components from other bacterial pathogens. Elucidating the mechanism of FlaA detection in human cells is important, and may lead to the identification of novel pathways of human innate immunity against microbes.

We are conducting co-infection experiments in mice. Mice are first infected with Influenza virus, and allowed to recover from weight loss before being challenged with *L. pneumophila* at a dose of $1x10^6$ intranasaly. The bacterial infection is allowed to proceed for up to four days, at which point the mice are sacrificed, and the outcome of infection is analyzed. We are checking for bacterial burden by monitoring the weight of the animals during the infection, enumerating total lung colony-forming units (cfu's), assaying for dissemination by checking for liver cfu's and analyzing the cell population in a bronchial-lavage fluid via FACS analysis, as well as studying cytokine release from lung cells. The described experiments are ongoing.

Aim 3: Completed during the previous reporting period.

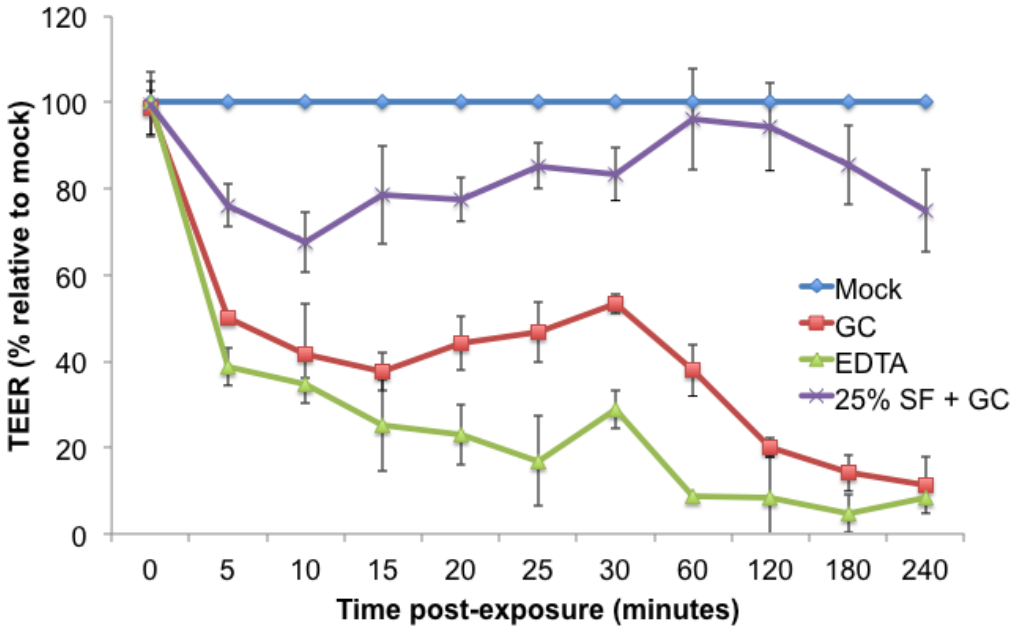

Fig. 1. Time-dependent reductions in epithelial TEER by *N. gonorrhoeae* are partially abrogated by the presence of seminal fluid. Ect1/E6E7 cells cultured in a transwell tissue culture system were maintained in cervicovaginal fluid simulant (CFS) or exposed to either *N. gonorrhoeae* in CFS or *N. gonorrhoeae* combined with seminal fluid (25%) in CFS for 4 hours at 37°C. TEER values were recorded at the indicated post-exposure times. TEER is expressed as a percent relative to TEER values for CFS-only, mock-exposed cells. SF, seminal fluid; GC, *N. gonorrhoeae.*

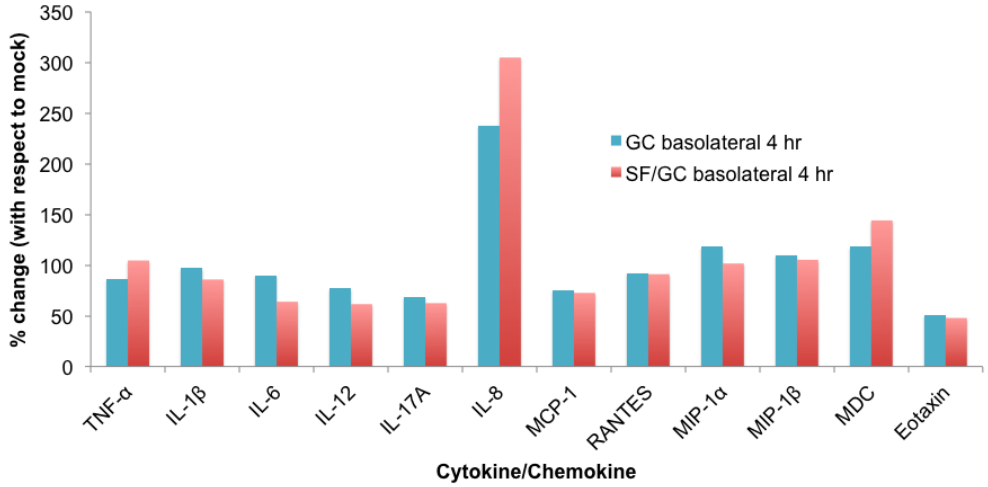

Fig. 2. *N. gonorrhoeae* and seminal fluid exposure causes an additive increase in basolateral IL-8 release. Ect1/E6E7 cells cultured in a transwell tissue culture system were maintained in cervicovaginal fluid simulant (CFS) or exposed to either *N. gonorrhoeae* in CFS or *N. gonorrhoeae* combined with seminal fluid (25%) in CFS for 4 hours at 37°C. Conditioned media samples from the basolateral chambers were analyzed for cytokine and chemokine content at 4 hours post-exposure. Analyte concentration is expressed as a percent relative to analytes detected in conditioned media from CFS-only, mock-exposed cells. SF, seminal fluid; GC, *N. gonorrhoeae.*

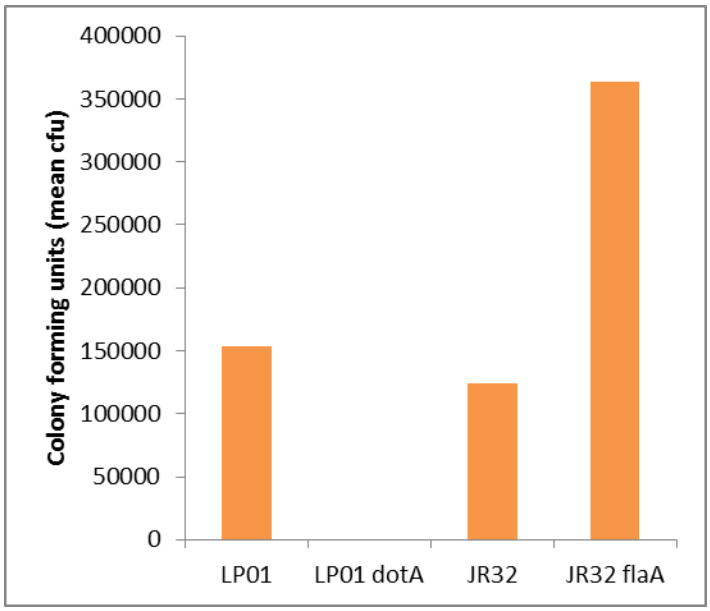

Fig 3. *L. pneumophila* replication inside of primary human monocyte-derived macrophages is partially restricted due to bacterial FlaA expression. *L. pneumophila* growth rates were determined in human monocyte - differentiated macrophages. Intracellular growth of wild type strains JR32 and LP01 was compared to that of an isogenic LP01 *dotA* mutant, and an isogenic JR32 *flaA* mutant. Each time point represents the mean number of viable bacteria recovered (mean cfu) from triplicate wells.

Research Project 8: Project Title and Purpose

Interaction of Interstitial Flow and ErbB2 Signaling in Breast Cancer Invasion – Interstitial fluid flow, which is the movement of fluid through tissues, increases in tumors and has been shown to promote tumor invasion, differentiation of stromal fibroblasts into myofibroblasts, increased cell motility, and activation of lymphatic endothelial cells. It is clearly evident that interstitial flow can have significant effects on tumor cells and their local microenvironment. However, there is a significant dearth of knowledge regarding how interstitial flow-induced cell signaling interacts with oncogenic signaling pathways to promote tumor invasion. Here, we propose a novel concept—that interstitial fluid flow mechanotransduction and ErbB2-activated signaling pathways cooperate to drive progression from premalignant to invasive cancer.

Anticipated Duration of Project

1/1/2013 – 12/31/2014

Project Overview

Based on preliminary evidence, we propose that the response of ErbB2+ breast cancer cells to interstitial flow is potentially a critical trigger in the transition from DCIS to invasive breast cancer. The objectives of this project are to demonstrate that interstitial fluid flow induces

invasion in ErbB2+ breast cancer cells, and determine what molecular factors mediate flow-induced invasion. *Our central hypothesis is that interstitial flow activation of chemokine receptors and phosphatidylinositol 3-kinase (PI3K) collaborates with ErbB2 signaling to enhance invasion of breast cancer cells.* We will utilize an *in vitro* three dimensional (3D) cell culture system developed in my laboratory that mimics DCIS phenotypes to unveil interstitial flow as a novel contributor to cancer progression and to test relevant potential therapeutic targets for blocking the invasion of breast cancer cells. To test this hypothesis, we propose three aims:

Aim 1—Determine the effects of interstitial fluid flow on ErbB2+ breast cancer cell invasion. We will characterize a flow invasion assay incorporating *in vivo*-like 3D cell structures and quantify the effects of interstitial fluid flow on breast cancer cells invasion.

Aim 2—Elucidate mechanisms of interstitial flow mechanotransduction in ErbB2+ breast cancer cells. Our initial focus will be on chemokine signaling and the role of PI3K. We will determine the role of chemokines in our system.

Aim 3—Measure changes of interstitial flow during tumor invasion in an *in vivo* breast cancer model. We will use MRI imaging to measure changes in interstitial flow to correlate with tumor progression in the mammary fat pad. These studies will begin to address the potential contribution of interstitial flow on cancer progression of ErbB2+ tumors *in vivo*.

Principal Investigator

Mauricio J. Reginato, PhD
Associate Professor
Drexel University College of Medicine
Department of Biochemistry & Molecular Biology
245 N. 15th Street, MS#497
Philadelphia PA 19102

Other Participating Researchers

Adrian Shieh, PhD; Alimatou Tchafa – employed by Drexel University
Sergey Karakashev – employed by Drexel University College of Medicine

Expected Research Outcomes and Benefits

The hypothesis underlying the proposed work is extremely innovative in current breast cancer research. The hypothesis is paradigm shifting and suggests that there is a connection between interstitial flow and progression from premalignant to malignant invasive ErbB2 positive breast cancers. There is great interest in understanding how premalignant breast cancer, such as ductal carcinoma in situ (DCIS) can progress to invasive breast cancer and how to predict risk of progression for each patient. The potential of interstitial flow to promote progression to invasive breast cancer has to our knowledge not been considered. Demonstration that treatment of DCIS models in vitro with increased interstitial flow results in development of traits of invasive breast cancer and identification of signaling pathways involved would create a field of study

concerning novel markers and potential targets for therapeutic intervention in breast cancer. Moreover, validation that increase in interstitial flow is associated with invasion and metastasis using in vivo model is novel and will be tested for the first time. Our work will yield important novel information on the potential contribution of interstitial flow to cancer associated signaling, as well as provide an intellectual basis for other researchers in the field of breast cancer signaling to examine relationships between interstitial flow and cancer invasion in their own systems related to understanding mechanisms of oncogenic progression and signaling.

Summary of Research Completed

Aim 2: Progress
Interstitial Fluid Flow (IFF) induces invasion of breast cancer cells through PI3-K activation.
To model non-invasive and invasive cells, we have developed a model system of breast cancer based on MCF-10A human mammary epithelial cells engineered to overexpress *ERBB2*: MCF-10A cells retrovirally transduced with either wild-type *ERBB2* (NeuN) or a constitutively active mutant of *ERBB2* (NeuT). When cultured in 3D conditions, NeuN cells exhibit behavior of pre-invasive *ERBB2* positive ductal carcinoma *in situ* (DCIS), while NeuT cells behave like *ERBB2* positive invasive ductal carcinoma (IDC). Using this 3D invasion assay, we observed a 2-fold increase in invasion in response to IFF in both NeuN and NeuT cells, as reported last year.

To determine the signaling pathways involved in the observed IFF-induced invasion, we examined pathways known to be important for cell invasion (ERBB2, MAPK, PI3K). We isolated cells from gels after the 3-D invasion assay and harvested protein from the resulting cells. Western blot revealed an increase of phosphorylated p85 (the regulatory subunit of class I PI3K complex) in both NeuN and NeuT cells treated with IFF (Fig. 1B).

These results were confirmed by treating other breast cancer cells overexpressing ERBB2/HER2 including SKBR3, BT474, and MDA-MB-453 with IFF. We demonstrated increased invasion coupled with increased PI3K phosphorylation compared to static condition (data not shown).

To test whether PI3K activity was required for IFF-induced invasion we treated cells with PI3K inhibitor LY294002 (a pan-PI3K inhibitor). Treatment with LY294002 decreased IFF-induced invasion in NeuN, NeuT (Fig. 1B and breast cancer cells SKB3 and MDA-MB-453 cells. Thus, this data suggests that IFF increases invasion in ERBB2 overexpressing breast cancer cells via activation of PI3K and requires its downstream signaling.

p110β modulates response to interstitial fluid flow in NeuT but not NeuN cells.
Class I PI3K is present in cells as a heterodimer complex made up of a regulatory (p85 or p101) and a catalytic subunit (p110). The catalytic subunit (p110) is responsible for propagating downstream signaling through its kinase activity. Using inhibitors that specifically target the β (TGX-221) or α (PIK-75) p110 catalytic subunit of PI3K, we observed that in NeuN cells, only cells treated with p110 inhibitor blocked IFF-mediated invasion (Fig. 2A). However in NeuT cells, inhibiting both α and β isoforms decreased IFF-induced invasion (Fig. 2B). NeuN and NeuT cells contained similar levels of p110α and p110β protein (Fig. 2C) thus ruling out altered levels of subunits for providing altered requirement for IFF-mediated invasion (Fig. 2C). Thus, NeuN and NeuT cells have divergent activation and requirement for p110 subunits in IFF-

mediated invasion.

CXCR4 regulates PI3K activity in response to interstitial fluid flow in NeuT cells.
Since previous studies have linked p110α to receptor tyrosine kinase signaling while p110β has been linked to G protein coupled receptors (GPCR), we investigated the role of GPCRs, and specifically chemokine receptors, in the IFF-induced invasion of NeuT cells. CXCR4 is a known modulator of breast cancer invasion and since IFF-induced invasion was previously shown to be dependent on CXCR4 we tested the role of CXCR4 on IFF-mediated invasion in ERBB2 expressing breast cancer cells. Treating NeuT cells with antagonists of the chemokine receptor CXCR4 (AMD3100 or WZ811) significantly reduced IFF-induced invasion (Fig. 3A). In contrast, AMD3100 and even pertussis toxin $G\alpha_i$ subunit inhibitor of all GPCRs treatment had no effect on IFF-mediated invasion in NeuN cells (Fig. 3B), suggesting that chemokine receptors, including CXCR4, are not involved in the molecular pathway activated by IFF in NeuN cells. CXCR4 inhibitors also had no effect on IFF-mediated invasion in the non-invasive HER2 positive cell line SKBR3 (data not shown).

To test whether CXCR4 signaling was associated with PI3K activation, we examined the effect of treating NeuT or NeuN cells with AMD3100 on p85 phosphorylation during IFF-mediated invasion. IFF-induced PI3K phosphorylation was decreased in NeuTs when the cells were treated with AMD3100 but phosphorylation was weakly inhibited in NeuN (Fig. 3C). Interestingly, total CXCR4 is expressed in both NeuN and NeuT at similar levels (Fig. 2). These data suggest that in NeuT cells a CXCR4 and its ligand CXCL12 may form a gradient that is required for IFF-mediated invasion. To test this idea, exogenous CXCL12 was added to the surrounding media and matrix at a uniform concentration of 80 ng/ml. Under these conditions NeuT cells no longer responded to IFF (CXCL12 condition) compared to a 2-fold increase in invasion in the control flow condition (Fig. 3D). These data suggest that NeuT cells, unlike NeuN cells, establish a gradient of CXCL12 that is necessary for IFF-induced activation of PI3K and invasion.

EMT confers a CXCR4 and p110 dependent IFF response in ErbB2-expressing cancer cells.
NeuN cells adopted more epithelial-like shapes on 2D cell culture plates and invaded in clumps of cells similar to their parental MCF10A counterparts (Figure 4B). However NeuT invaded as single cells. Thus, we hypothesized that NeuT cells may have undergone EMT. To test this idea, we probed for protein expression of epithelial markers, and observed loss of E-cadherin and increased levels of vimentin in NeuT cells when compared to NeuN cells (Fig. 4 A, B). Both of these proteins are known markers of EMT. We examined gene differences between NeuN and NeuT cells further, using microarray analysis of known EMT-associated genes that revealed significant differences when comparing NeuT and NeuN mRNA expression. The expressions of all these genes agree with published EMT-associated data. We validated the microarray result with quantitative RT-PCR of three of the identified genes. Taken together, these data further support the idea that NeuT cells display a more mesenchymal-like phenotype when compared to NeuN cells.

To determine whether EMT contributes to the altered IFF response, EMT was induced in NeuN cells using the known EMT inducing growth factor TGF-β1. The cells were treated for 6 days with 20ng/ml TGF-β1 and EMT induction was confirmed using western blot and immuno-

fluorescence. NeuN^{EMT} show lower levels of E-cadherin and higher levels of vimentin when compared to their control NeuN counterparts (Fig. 4 C, D). As expected, the NeuN cells induced to undergo EMT had higher levels of basal invasion (Fig. 5B). However, in line with our previous findings on NeuT cells, we observe that IFF-induced invasion in NeuN^{EMT} became sensitive to pan-chemokine receptor inhibitor (pertussis toxin; Fig. 5A) , and CXCR4 inhibitor (AMD3100) compared to untreated cells (Fig. 5B). In addition, IFF-induced PI3K phosphorylation in the presence of AMD3100 was significantly reduced (Fig. 5C) in NeuN^{EMT} cells similarly to that seen in NeuT cells (Fig. 3C). Consistent with these results, treatment of NeuN^{EMT} cells with p110β inhibitor (TGX221) reduced IFF-mediated invasion unlike their normal counterpart (Fig. 5D) but similar to NeuT cells (Fig. 3). Thus, these data support the hypothesis that EMT alters IFF-mediated invasion to a CXCR4- and p110-dependent manner in ErbB2 expressing breast cancer cells.

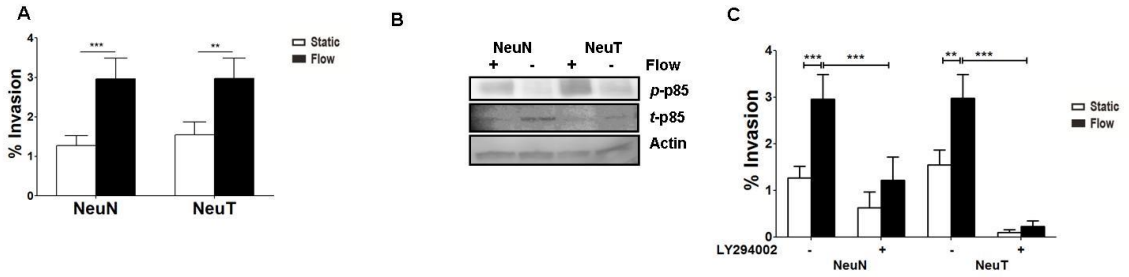

Figure 1. Figure 1: IFF-induced invasion occurs through p85 activation. A) IFF increases invasion of NeuN and NeuT. Percent invaded cells after 24 hours in 3-D IFF assay. All values are mean ± SEM. Student t test (*: $p < 0.05$; **: $p < 0.01$, ***: $p < 0.001$), n>12. B) IFF induces activation of PI3K in NeuN and NeuT. Representative western blot of phosphorylation of PI3K regulatory subunit (p85) after 24 hours of static or flow conditions in 3D flow invasion assay; β actin was used as loading control. C) PI3K activity is necessary for IFF-induced invasion in both cell lines. IFF-induced invasion is decreased in the presence or absence of LY294002, a pan PI3K inhibitor. All values are mean ± SEM. Student t test and 2-way ANOVA (*: $p < 0.05$; **: $p < 0.01$, ***: $p < 0.001$), n>6.

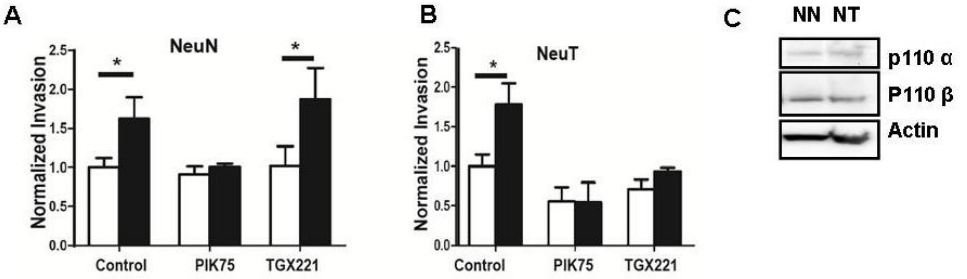

Figure 2: Separate p110 isoforms are necessary for IFF induced invasion in NeuN and NeuT. A-B) Both p110α and p110β are necessary for flow response in NeuT only. Cellular response to P110 isoforms specific inhibitors PIK75 and TGX221 (p110α and p110β inhibitors respectively) in NeuN (A) and NeuT (B). All values are mean ± SEM. Student t test (*: $p < 0.05$. *: $p < 0.05$; **: $p < 0.01$, ***: $p < 0.001$), n=6. C) Both cells express similar levels of p110 isoforms. Representative western blot of p110α and β in NeuN and NeuT; β actin was used as loading control.

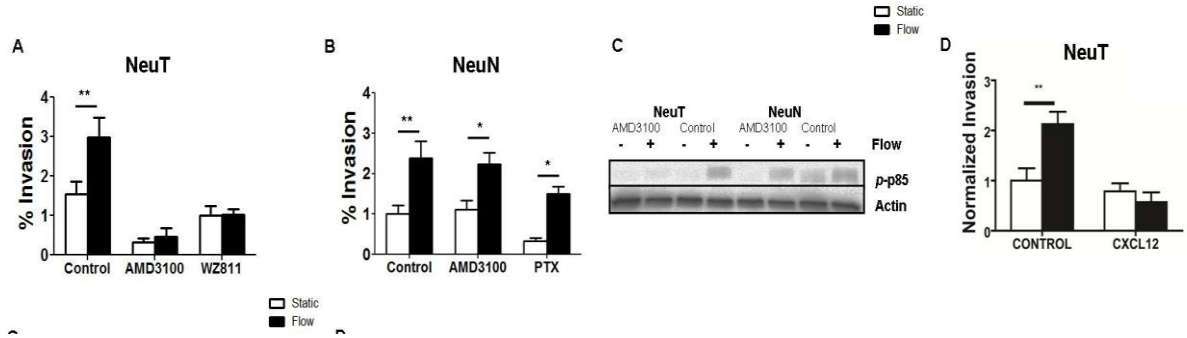

Figure 3: CXCR4 activity is required for IFF induced invasion in NeuT but not NeuN. A) Changes in invasion in the presence or absence of CXCR4 inhibitors (AMD3100 and WZ811) in NeuT. B) AMD3100 and pertissus toxin are not necessary for IFF-induced invasion in NeuN. C) AMD3100 inhibits IFF-induced PI3K activation in NeuT but not n NeuN. Representative western blot of phospho-p85 after 24 hours in 3D invasion assay with and without the inhibitor in NeuN and NeuT; β actin was used as loading control. D) Changes to flow induced invasion when exogenous CXCL12 is added to surrounding matrix and media. NeuT respond to fluid flow only in the presence of a CXCL12 gradient. All values are mean ± SEM. Student t test (*: $p < 0.05$. *: $p < 0.05$; **: $p < 0.01$, ***: $p < 0.001$); n>6.

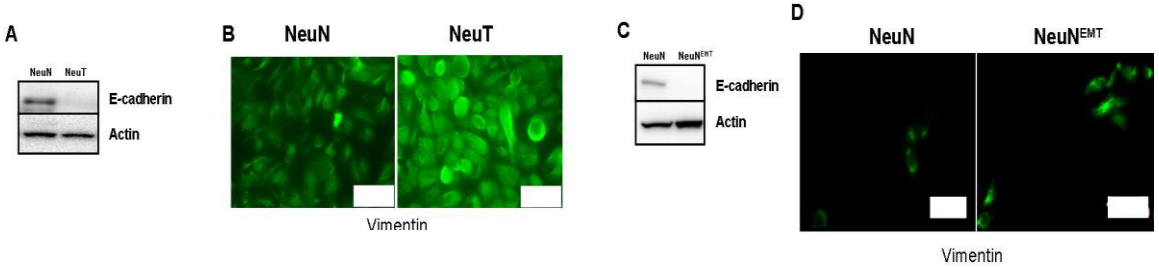

Figure 4: NeuT cells have undergone EMT similar to TGF-b1 dependent EMT induction in NeuN. A.) compared to NeuN, NeuT cells express lower levels of epithelial markers. Representative vestern blot of E- cadherin; b actin was used as loading control. B.) Compared to NeuN, NeuT cells express higher levels of mesenchymal markers. Representative immunofluorescence of vimentin from cells plated on collagen I coated cover-slip. C.) Compared to control, $NeuN^{EMT}$ cells express lower levels of epithelial markers. Representative vestern blot of E- cadherin; bactin was as loading control. D.) Compared to control, $NeuN^{EMT}$ cells express higher levels of vimentin. Representative immunofluorescence of vimentin from cells attached to the underside of membrane after IFF invasion assay. White bar represents 50mm.

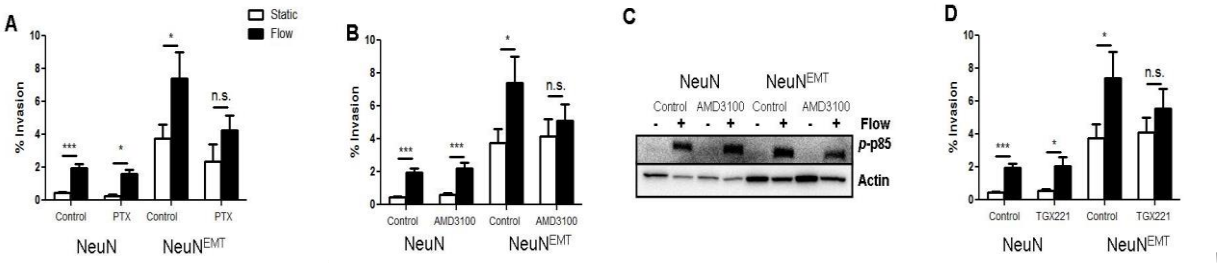

Figure 5: TGFβ1-induced EMT in NeuN leads to CXCR4 and p110beta dependent IFF response. A) Changes in invasion in the presence or absence of pertussis toxin. Inhibiting GPCR activity in $NeuN^{EMT}$ blocks IFF-induced invasion but not in control NeuN. B) Changes in invasion in the presence or absence of CXCR4 inhibitors, AMD3100. Inhibiting CXCR4 activity in $NeuN^{EMT}$ blocks IFF-induced invasion but not in control NeuN. C) AMD3100 decreases IFF-induced PI3K activation in $NeuN^{EMT}$ but not in control. Representative western blot of phospho-p85 after 24 hours in 3D invasion assay with and without the inhibitor; β actin was used as loading control. D) Changes in invasion in the presence or absence of p110β inhibitors, TGX221. Inhibiting CXCR4 activity in $NeuN^{EMT}$ blocks IFF-induced invasion but not in control NeuN. All values are mean ± SEM. Student t test (*: $p < 0.05$. *: $p < 0.05$; **: $p < 0.01$, ***: $p < 0.001$); n>6.

Research Project 9: Project Title and Purpose

An Analysis of Mitochondrial Mutation and HIV Antiretroviral Therapy – This project will examine the potential for mitochondrial changes to be used to predict clinical outcomes in HIV positive patients.

Anticipated Duration of Project

1/1/2013 – 12/31/2014

Project Overview

We have developed a novel approach to the analysis of changes in the mitochondria which offers potentially novel insights into the effect of antiretroviral therapy (ART) on mitochondrial function and may provide a rapid screen to identify patients most at risk for neurocognitive decline. Our object was to identify an approach which will allow us to quantify the relative susceptibility of an individual to ART. We have identified mitochondrial mutations associated with ART and we predict that this increased mutation rate represents an increased intrinsic susceptibility to therapy. Further, we predict that patients exhibiting this phenotype are more likely to suffer neurocognitive decline with age and continued antiretroviral therapy.

Given this background, we propose to examine the mitochondrial mutation rate in patients being cared for in the Drexel University College of Medicine HIV/AIDS clinic, located in Philadelphia, Pennsylvania, USA and correlate the mutation rate with neurocognitive function in these patients using a battery of neurocognitive analyses that specifically test prefrontal dementia.

Specific Aims:

1A. Perform a retrospective analysis of mitochondrial mutations in two defined regions of the mitochondrial genome using DNA samples derived from patients enrolled in the Drexel University College of Medicine HIV/AIDS Genetic Analysis Cohort.

1B. Perform a longitudinal analysis of mitochondrial mutations in patients enrolled in the Drexel University College of Medicine HIV/AIDS Genetic Analysis Cohort.

Principal Investigator

Christian Sell, PhD
Associate Professor
Department of Pathology, Room 5605
Drexel University College of Medicine
245 N 15th Street
Philadelphia, PA 19102

Other Participating Researchers

David Libon, PhD; Brian Wigdahl, PhD; Mike Nonnemacher, PhD; Vanessa Pirrone, PhD; Jeffery Jacobson, MD; Claudio Torres, PhD – employed by Drexel College of Medicine

Expected Research Outcomes and Benefits

The project will provide the ability to tailor individual therapy for antiretroviral drugs based upon the patient's susceptibility to these drugs. This will help to limit the long-term impact of antiretroviral therapy on patient health.

Summary of Research Completed

Aim 1A: Progress

A total of 434 patients have been enrolled into the DREXELMED HIV/AIDS Genetic Analysis Cohort to assess the role that genetic variation within the HIV-1 sequence plays in disease progression and potentially in the development of neurological complications. We collected blood from these 434 patients for drug testing and viral genetic assessment and determined clinical parameters for each patient at each visit. A total of 869 visits have been completed since the start of the project. Samples have been obtained from patients that are both naive to ART and are currently receiving ART and the level of compliance has been evaluated. Peripheral blood mononuclear cell DNA samples were obtained from the DrexelMed/HIV Genetic Analysis cohort. Due to the fact that the cohort has been followed longitudinally for several years, it was possible to obtain matched samples obtained at first visit when patients were naive to therapy and following 1.5-2 years of ART.

To examine changes in the mitochondrial genome, 2 fragments, one including a portion of the D loop region (bp14898-151 of the Cambridge reference sequence) and one including a portion of the mitochondrial cytochome C oxidase gene (bp 8910-10648), were amplified from 3 patients using primer sets that have been verified to amplify the mitochondrial genome exclusively and have no cross reactivity with nuclear DNA. Interestingly, a very similar approach using one variable region and one coding region of the mitochondrial genome has been recently reported by the Chinnery group in the UK for the analysis of very low levels of heteroplasmy within the human population. The DNA fragments resulting from the amplification of these 2 regions in our patients were subjected fragmentation, library construction and deep sequence analysis using the Illumina Solex platform. Greater than 20,000 fold coverage was obtained with 1.4 to 2.3 $x10^6$ reads per sample at 94% high quality reads (Q value 38.8 or higher).

An increase in C/G/T to A transition/transversion was observed in all patient samples following initiation of ART. Interestingly, in only 1 patient was there a corresponding increase in C/G/A to T transitions/transversions, suggesting that the incorrect DNA base was not removed (difference in T substitutions P=0.0005). This suggests that this patient is less able to remove the nascent mismatch bases and will be at higher risk for HIV associated neurocognitive dementia or HAND. Consistent with this interpretation is the fact that the vast majority of adenosine mismatches correspond to cytosine residues in the Cambridge reference sequence while thymidine

mismatches correspond to guanine residues in the Cambridge reference sequence. These changes are logical when one considers the fact that a cytosine chain terminator analog (emtrieitibine) is part of the ART that these patients received. Thus, it appears that the adenosine mismatches are a direct result of the presence of the cytosine chain terminator analog used in therapy while the thymidine mismatches from the Cambridge reference sequence represent mutations that have been replicated and are now incorporated into the mitochondrial genome in a subpopulation of the mitochondrial DNA present in the cell. These are remarkable findings, both because we are able to detect nascent DNA damage due to the NRTIs and because we have found variation in the response to this damage. Our ability to detect these mutation rates is due to the high degree of coverage in the sequencing approach. We obtained greater than 20,000 fold coverage for the genome segments analyzed combined with a high quality of sequence data. With this depth of coverage we are able to detect both the error rate of the polymerase gamma enzyme and the subsequent mutations resulting from these errors while previous studies have not been powered to detect errors and mutations at this level and thus have not reported these differences. These results open a new window into the influence of NRTIs on mitochondrial dynamics.

A) Mitochondrial Haplogroup Analysis

Recent studies have uncovered a relationship between the individual's mitochondrial haplogroup and HIV progression, the risk for Alzheimer's disease. In addition an analysis of patients in the CHARTER study revealed a decreased incidence of peripheral neuropathy in patients with the European mitochondrial haplogroup J and the African subgroup L1c receiving HAART. We are determining the mitochondrial haplogroup for the 39 patients who have undergone the neurocognitive evaluation procedure developed by Dr. Libon. Additional patients who undergo the neurocognitive evaluation will also be screened for mitochondrial haplogroup, circulating mitochondrial DNA, and will be evaluated for mitochondrial mutation rate. This effort will provide a growing database that includes neurocognitive evaluation and a variety of mitochondrial markers. This database will be used both to identify correlations within the DrexelMed HIV/AIDS Genetic Analysis Cohort but also as a resource for comparisons with other HIV/AIDS cohorts such as the CHARTER (CNS HIV Antiretroviral Therapy Effects Research) study.

Aim 1B: Progress

B) Circulating mitochondrial DNA

Several studies have suggested that the level of mitochondrial DNA present in the plasma may be reflective of mitochondrial stress, inflammatory status and clincial outcome in trauma. For this reason, we have examined ciculating levels of mitochondrial DNA as a second approach to examine the relative sensistivity to mitochondrial stress induced by ART. We have examined circulating levels of mitochondrial DNA in 39 patients who have undergone neurocongitive evaluation.

C) Neurocognitive evaluation

Neurocognitive impairment is thought to be present in 30 percent of asymptomatic and 50 percent of symptomatic HIV patients. The brain is a frequent target in HIV infection. Moreover, specific brain regions may be particularly susceptible to HIV infection including cortical white matter tracts and the basal ganglia. Recent data documents reduced basal ganglia volume using MRI in HIV patients. Reduced volume of the basal ganglia has been linked to slowness on tests

assessing motor, processing speed, and selected executive tests. Using proton magnetic resonance spectroscopy (MRS) Paul and co-workers, found reduced basal ganglia volume in cognitively impaired HIV patients. Dr. David Libon of the Drexel University School of Medicine and colleagues with the Temple University Psychology program have begun analyzing neurocognitive function in the DREXELMED HIV/AIDS Genetic Analysis Cohort. This evaluation is part of an ongoing collaboration and is supported by funds other than the current CURE proposal and no commonwealth funds have been used for the analysis. However, the results are pertinent to the current CURE project because the analysis provides detailed information regarding neurocognitive changes associate with HIV and ART as the population ages and permits a preliminary assessment of the utility of utilizing mitochondrial DNA markers as genetic tools to predict those individuals more prone to development of neurocognitive impairment during the course of disease.

Recent diagnostic criteria for HIV-related mild neurocognitive disorder (MND) suggests assessment of a wide range of neurocognitive cognitive operations including graphomotor/ processing speed, attention/working memory, executive control; declarative memory; language; and visuospatial operations. Wendelken and Valcour summarized a number of studies suggesting that older HIV-1 patients present with a pattern of neurocognitive deficits including psychomotor slowing; impairment in attention and executive functions; a mixed encoding/ retrieval pattern of impairment; but comparatively less difficulty in visuospatial and semantic operations. Using the protocol of neuropsychological tests described below, five neurocognitive indices are calculated. In the initial analysis, the association between mutation burden as a binary function (presence of mutations, yes or no) and neurocognitive functions are assessed with a series of multiple regression analyses relative to a measure of projected general cognitive abilities (i.e., single word reading ability; WRAT-IV Reading subtest) as the dependent variable. Power analysis base to detect a deviation of 0.5 SD from the norm on the neurocognitive status protocols reveals a need for 52 patients in each group, with or without mutation. Age and status will be entered into the analysis in the second block and a simple analysis of the cognitive status relative to the presence or absence of mutations will be performed. Initial analysis is performed on patients with undetectable viral loads and CD4 counts over 500. In subsequent blocks variables such a viral burden and drugs of abuse are examined as co-variables. The neurocognitive protocol for this research is listed below.

Working Memory/ Mental Search: *Neuropsychological Assessment Battery – Digit Span subtest*: The dependent variables include age-corrected scale score for digits forward and backwards. *Letter fluency (letters FAS*) – The dependent variable is an age/ education-corrected scale score. Response Inhibition **:** *Number Interference (Stroop) Test*. This test is based on the classic Stroop paradigm. Participants are required to inhibit a pre-potent response set. This version of the Stroop Test consists of three test conditions, each consisting of 6 blocks of 10 trials. Outcome measures for each test condition are total time to completion, errors within each trial block, and total errors. Condition 1 (baseline) – participants are asked to solve simple single digit multiplication or addition problems (e.g., 7 + 4; 9 x 3). Six blocks of 10 problems are presented. Condition 2 (inhibition) – the contingencies of the test are changed so that when participants see an addition problem they are now required to multiple, when shown a multiplication problem they are required to add. Condition 3 (inhibition/ switching) – consists of four types of stimuli – (a) when shown an addition problem participants are asked to multiply (as in condition 2); (b)

when shown an addition problem inside a box participants are asked to add (as in condition 1); (c) when shown a multiplication problem participants are asked to add (as in condition 2); (d) when shown a multiplication problem inside a box participants are asked to multiply (as in condition 1).
Processing Speed/ Visuoconstruction***:*** *WAIS-III Digit Symbol* – The dependent variable is an age-corrected scale score. *Complex Figure Copy* – The dependent variable is the age corrected scale score.
Lexical Retrieval/ General Intellectual Functions: *Animal Fluency* (6) – The dependent variable is the age-corrected scale score. *The Boston Naming Test* The outcome variable is the age-correct scale score.
Memory and Learning: *The California Verbal Learning Test-II (CVLT-II) – Memory is assessed with the CVLT-II*. The dependent variables will be total delay free recall and the recognition discriminability index.

A total of 39 patients have undergone the comprehensive neurocognitive evaluations established by Dr. Libon and colleagues. This ongoing effort will allow us to evaluate mitochondrial damage, mitochondrial DNA, and mitochondrial haplogroups as correlates to neurocognitive status.

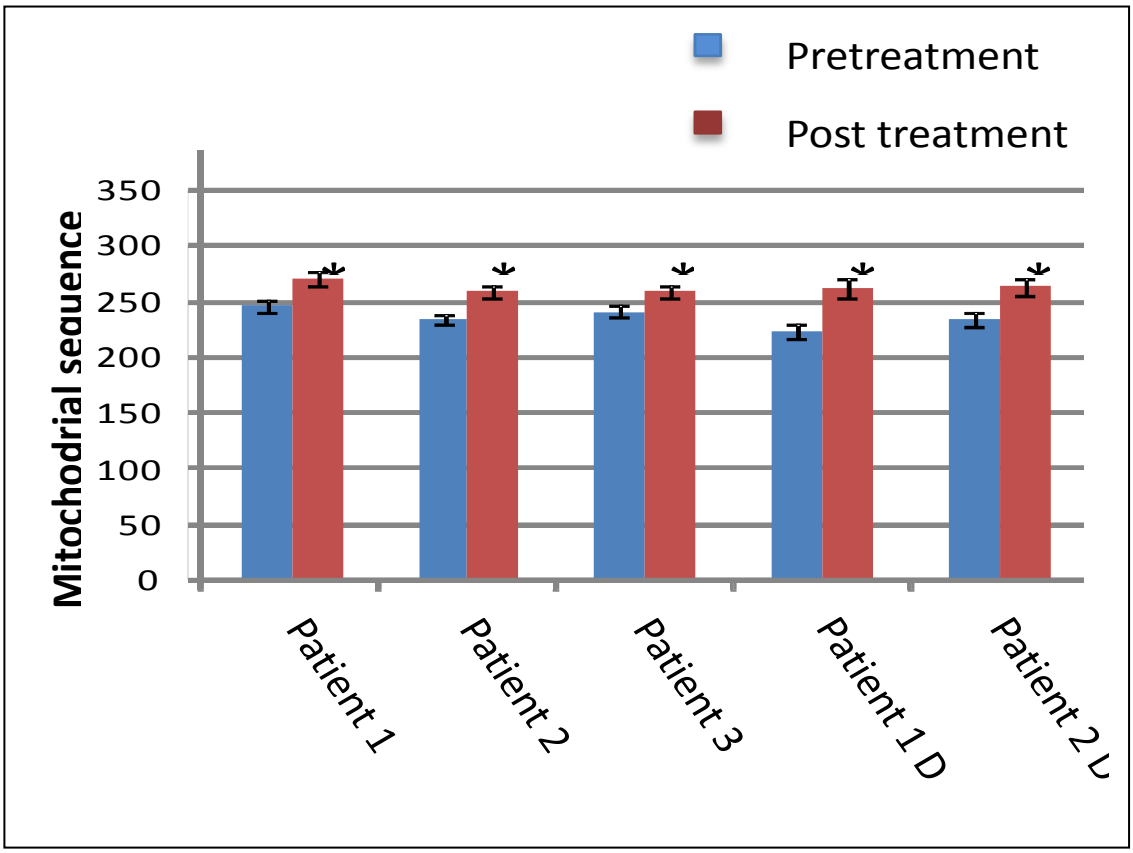

Figure 1. *Mitochondrial nucleotide error rate in patient samples following ART.*
Human DNA samples extracted from peripheral blood mononuclear cells (PBMCs) from patients naïve to ART and following 1.5 years of ART therapy were subjected to PCR amplification using primer sets that had been validated for specific amplification of the mitochondrial genome without amplification of the nuclear genome [3]. Two regions of the mitochondrial genome were chosen for amplification, the D loop region including a portion of hypervariable region 1 and a portion of the cytochrome oxidase coding region. The resulting DNA fragment we purified and subjected to library production and deep sequence analysis using an Illumina Genome Analyzer platform. Differences between pre and post treatment are significant at $P<0.001$ and are marked by an asterisk. The D loop sample from Patient 3 failed quality testing upon sequencing due to a technical consideration and is not presented for this reason.

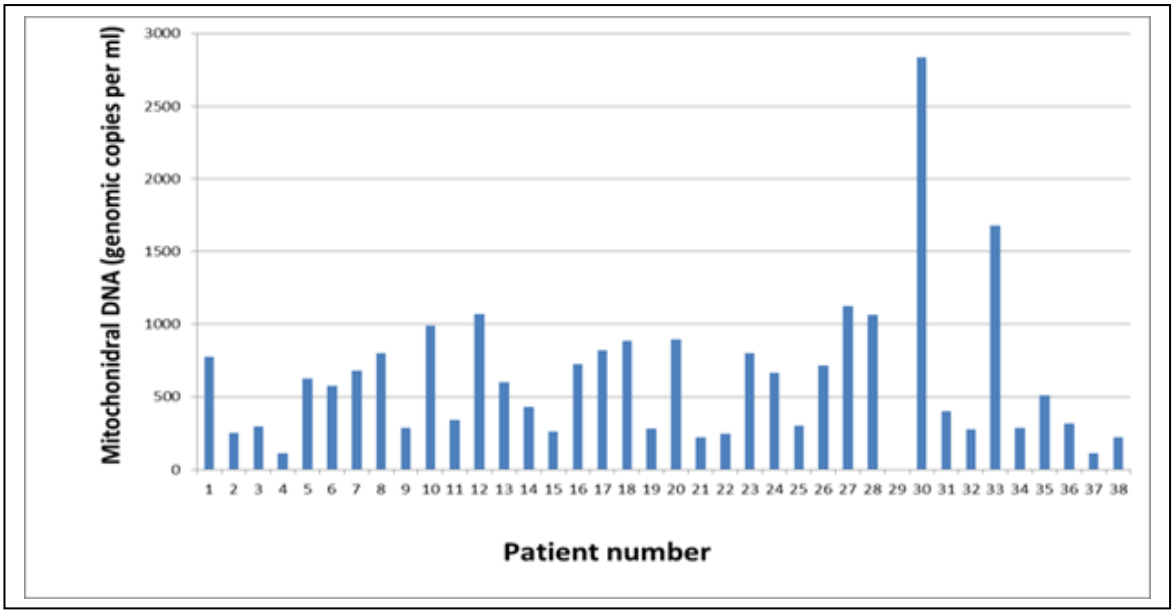

Figure 2. *Circulating mitochondrial DNA in the DrexelMed HIV/AIDS Genetic Analysis Cohort.* Quantitiative real-time PCR analysis of mitochondrial DNA content was performed on plasma samples from 39 patients in the DrexelMed HIV/AIDS Genetic Analysis Cohort using primers specific for the t-RNA leucine gene of the mitochondrial genome following our published technique. A plasmid carrying a fragment of the mitochondrial genome containing the t-RNA leucine gene was used as a calibrator allowing a precise quantification of mitochondrial DNA copy number in each patient.